bioRxiv preprint doi: https://doi.org/10.1101/2020.10.15.340612; this version posted October 15, 2020. The copyright holder for this preprint (which was not certified by peer review) is the author/funder, who has granted bioRxiv a license to display the preprint in perpetuity. It is made available under aCC-BY-NC-ND 4.0 International license.

Systematic analysis of innate immune antagonism reveals vulnerabilities of SARS-CoV-2

Manuel Hayn*[1], Maximilian Hirschenberger*[1], Lennart Koepke*[1], Jan H Straub[1], Rayhane Nchioua[1], Susanne Klute[1], Caterina Prelli Bozzo[1], Wasim Aftab[3,4], Fabian Zech[1], Carina Conzelmann[1], Janis A Müller[1], Smitha Srinivasachar Badarinarayan[1], Christina M Stürzel[1], Ignasi Forne[3], Steffen Stenger[5], Karl-Klaus Conzelmann[2], Jan Münch[1], Daniel Sauter[1], Axel Imhof[3], Frank Kirchhoff[1] and Konstantin MJ Sparrer[1]

*contributed equally, in alphabetical order.

Affiliations:

1 Institute of Molecular Virology
Ulm University Medical Center
89081 Ulm, Germany

2 Gene Center & Max von Pettenkofer-Institute of Virology
Ludwig-Maximilians-University of Munich
81377 Munich, Germany

3 Biomedical Center, Zentrallabor für Proteinanalytik (Protein Analysis Unit)
Department of Molecular Biology,
Ludwig-Maximilians-University of Munich
82152 Planegg-Martinsried, Germany

4 Graduate School for Quantitative Biosciences (QBM)
Ludwig-Maximilians-University of Munich
81377 Munich, Germany

5 Institute for Medical Microbiology and Hygiene
Ulm University Medical Center
89081 Ulm, Germany

Correspondence: Konstantin.Sparrer@uni-ulm.de

Running Title: Interplay between innate immunity and SARS-CoV-2

KEYWORDS: Innate Immunity, Autophagy, Interferon, SARS-CoV-2, SARS-CoV-1

bioRxiv preprint doi: https://doi.org/10.1101/2020.10.15.340612; this version posted October 15, 2020. The copyright holder for this preprint (which was not certified by peer review) is the author/funder, who has granted bioRxiv a license to display the preprint in perpetuity. It is made available under aCC-BY-NC-ND 4.0 International license.

ABSTRACT

The innate immune system efficiently defends the human host against viral pathogens. Thus, viruses evolved strategies to counteract immune activation. Here, we systematically analysed the impact of 29 SARS-CoV-2 encoded proteins on three major arms of our cell-intrinsic innate immune defences: interferon (IFN) induction, cytokine signalling and autophagy. Subsequent mechanistic analyses revealed that SARS-CoV-2 proteins target the respective signalling cascades at multiple steps. For example, we show that Nsp14 reduces endogenous IFN receptor levels and ORF3a and ORF7a perturb the late endosomal/trans-Golgi network. Our data demonstrates that most antagonistic activities are conserved between proteins encoded by SARS-CoV-2, the closely related bat RaTG13-CoV and the highly pathogenic SARS-CoV-1. However, SARS-CoV-1 Nsp15 is strikingly more potent in suppressing IFN induction and signalling than its SARS-CoV-2 counterpart. This may help explain the lower pathogenicity of SARS-CoV-2, which facilitated its rapid spread. Overall our analyses revealed that IFN-γ and IFN-λ1 signalling are antagonised the least, leaving SARS-CoV-2 highly susceptible to these two cytokines. Their combination synergistically potentiated the anti-viral effects against SARS-CoV-2 at low concentrations. Taken together, our results allow an explanation for differences in susceptibility towards IFNs and provide evidence that rational immune activation may be an effective future therapeutic strategy against SARS-CoV-2. (200 words)

bioRxiv preprint doi: https://doi.org/10.1101/2020.10.15.340612; this version posted October 15, 2020. The copyright holder for this preprint (which was not certified by peer review) is the author/funder, who has granted bioRxiv a license to display the preprint in perpetuity. It is made available under aCC-BY-NC-ND 4.0 International license.

INTRODUCTION

The severe acute respiratory syndrome coronavirus 2 (SARS-CoV-2) is a zoonotic, novel coronavirus that emerged at the end of 2019[1–3]. Infection with SARS-CoV-2 causes coronavirus disease 2019 (COVID-19)[4]. The virus rapidly spread all over the world owing to its higher transmission rates[5] (R=2.5), as well as a lower morbidity and case fatality rates (CFR 3-4%)[6] compared to previous epidemic coronaviruses like SARS-CoV-1 (R=2.0, CFR 11%) or MERS-CoV (R=0.9, CFR 35%)[7–9]. However, its pathogenicity is still much higher than that of 'common cold' CoVs such as HKU1 and 229E[10] and to date SARS-CoV-2 has caused more than a millions deaths (https://coronavirus.jhu.edu/map.html).

Upon infection of a target cell, CoVs are recognised by innate immune sensors, for example via RIG-I-like receptors (RLRs)[11], which activate cell-intrinsic innate immune defences (hereafter referred to as the innate immune system)[12,1314]. However, the exact ligand triggering the response is unknown. Activation of RLRs induces signalling cascades that ultimately lead to the release of IFNs and other pro-inflammatory cytokines as well as induction of anti-viral effectors[15]. Released cytokines are subsequently also recognised by neighbouring cells and induce an antiviral transcriptional response. Thus, both the infected cell and non-infected neighbouring cells are set in an anti-viral state[16,17] eventually limiting viral spread. Other branches of the innate immune system, such as autophagy, are activated during CoV infections as well[18,19]. Autophagy is capable of targeting viral components or even whole viruses for lysosomal degradation[20,21] and SARS-CoV-2 has evolved to block autophagic turnover[18]. Eventually activation of innate immunity recruits and stimulates the adaptive immune system ultimately facilitating elimination of the virus[22,23]. Notably, inborn defects in innate immunity or auto-antibodies against IFNs are associated with high frequencies of severe COVID-19 cases, suggesting that innate defence mechanisms play a major role in immune control of SARS-CoV-2[24,25]. SARS-CoV-2 infections show higher numbers of subclinical, asymptomatic infections (up to 80%[6]) compared to previous epidemic CoVs such as SARS-CoV-1[10]. Indeed, recent evidence suggests that SARS-CoV-2 can be more efficiently antagonised by IFNs than SARS-CoV-1 *in vitro*[26]. However, the

bioRxiv preprint doi: https://doi.org/10.1101/2020.10.15.340612; this version posted October 15, 2020. The copyright holder for this preprint (which was not certified by peer review) is the author/funder, who has granted bioRxiv a license to display the preprint in perpetuity. It is made available under aCC-BY-NC-ND 4.0 International license.

underlying reasons for differences in IFN susceptibility between SARS-CoV-2 and SARS-CoV-1 are currently not fully understood.

Recent reports demonstrated that infection with SARS-CoV-2 induces an imbalanced innate immune response, indicating manipulation by SARS-CoV-2[27,28]. Proteomics analysis of selected SARS-CoV-2 proteins revealed that innate immune activation is perturbed on multiple levels[27]. For example, it was suggested that ORF3a inhibits autophagic turnover, ORF8 alters Integrin-TGFβ-EGFR-RTK signalling[27] and ORF3b antagonises type I IFN induction by a yet unknown mechanism[29]. In addition, the SARS-CoV-2 non-structural protein 1 (Nsp1) shuts down cellular translation including the cytokine-mediated innate immune response[30]. Analysis of the interplay between SARS-CoV-2 proteins and IFN-β induction and signalling revealed that at least eight SARS-CoV-2 proteins interfere with type I IFN signalling[31,32]. Among them is ORF6, which was suggested to interfere with nuclear trafficking of transcription factors thereby impairing gene induction[32,33]. However, so far only type I IFN signalling was analysed in some detail and our knowledge how SARS-CoV-2 manipulates innate immunity is far from being complete.

Currently, treatment with IFNs is explored in clinical trials against SARS-CoV-2[34]. However, patients receiving immunomodulatory therapy with IFNs generally suffer from severe side-effects including psychological symptoms such as depression[35–37]. Novel strategies which activate the immune system but reduce inflammation and lower doses of cytokines are required[38]. Thus, analysing how SARS-CoV-2 antagonises innate immunity may give valuable clues on viral vulnerabilities that might be exploited for effective and safe therapeutic immune control.

Here, we systematically analysed the impact of 29 SARS-CoV-2 encoded proteins[29,39,40] on the major branches of the cell-intrinsic innate immune system: IFN induction, IFN/pro-inflammatory cytokine signalling and autophagy. This identified Nsp1, Nsp3, Nsp5, Nsp10, Nsp13, Nsp14, ORF3a, ORF6, ORF7a and ORF7b as the major innate immune antagonists encoded by SARS-CoV-2. Interference with innate immune activation is achieved by using a diverse, synergistic set of mechanisms ranging from downregulation of IFN receptor expression by Nsp14 to blockage of autophagy via fragmentation of the trans-Golgi network by the viral proteins ORF3a and ORF7a. Strikingly, our data indicate that

bioRxiv preprint doi: https://doi.org/10.1101/2020.10.15.340612; this version posted October 15, 2020. The copyright holder for this preprint (which was not certified by peer review) is the author/funder, who has granted bioRxiv a license to display the preprint in perpetuity. It is made available under aCC-BY-NC-ND 4.0 International license.

Nsp15 of both RaTG13-CoV and SARS-CoV-2 counteract type I IFN induction and signalling much less efficiently than SARS-CoV-1 Nsp15. Our analyses of SARS-CoV-2 mediated counteraction of IFN signalling revealed that IFN-γ and IFN-λ1 pathways are antagonised the least, and consequently treatment with these two cytokines is most potent against SARS-CoV-2. Combined IFN treatment at very low doses potentiates the individual anti-viral effect and can be further improved by anti-inflammatory autophagy activation. Thus, our results provide a plausible explanation why SARS-CoV-2 is more susceptible against IFN treatment than SARS-CoV-1 and indicate that combination of IFN-γ and IFN-λ1 is an effective anti-SARS-CoV-2 approach.

RESULTS

A variety of SARS-CoV-2 proteins antagonise innate immune pathways

To systematically examine how SARS-CoV-2 manipulates innate immunity, we used Strep II-tagged expression constructs[39] coding for 28 of the 30 currently reported SARS-CoV-2 proteins (Nsp1, Nsp2, Nsp4, Nsp5, Nsp6, Nsp7, Nsp8, Nsp9, Nsp10, Nsp11, Nsp12, Nsp13, Nsp14, Nsp15, Nsp16, S, ORF3a, ORF3c, E, M, ORF6, ORF7a, ORF7b, ORF8, ORF9b, N, ORF9c and ORF10) (Fig. 1a). In addition, we examined untagged Nsp3. Expression of all proteins was confirmed by western blotting (Supplementary Fig. 1a) and immunofluorescence analyses (Supplementary Fig. 1b). The impact of all 29 viral proteins on three major branches of innate immunity: IFN/pro-inflammatory cytokine induction via RLRs (Fig. 1b, Supplementary Fig. 1c), signalling (Fig. 1c, Supplementary Fig. 1d) and autophagy (Fig. 1d, Supplementary Fig. 1e) was analysed by quantitative reporter assays.

Induction of type I IFNs (IFN-α and IFN-β) was monitored using a Firefly luciferase reporter controlled by the full IFN-α4 promotor, the full IFN-β promoter, or isolated binding sites for the transcription factors IRF3 or NF-κB (Fig. 1b). All assays were normalized for cell viability (Supplementary Fig. 1f). HEK293T cells were infected with Sendai Virus, mimicking RLR activation by SARS-CoV-2. Nsp2, Nsp6 and Nsp12 slightly enhanced both IFN-α4 and IFN-β promoter induction as well as IRF3-dependent transcription (Fig. 1b). However, our analyses revealed that Nsp1, Nsp3, Nsp5, Nsp10,

bioRxiv preprint doi: https://doi.org/10.1101/2020.10.15.340612; this version posted October 15, 2020. The copyright holder for this preprint (which was not certified by peer review) is the author/funder, who has granted bioRxiv a license to display the preprint in perpetuity. It is made available under aCC-BY-NC-ND 4.0 International license.

Nsp13, ORF6 and ORF7b are the major SARS-CoV-2 encoded antagonists of type I IFN induction (Fig. 1b).

Treatment with type I and III IFNs, such as IFN-α, IFN-β and IFN-λ1 culminates in the induction of genes with IFN response element (ISRE)-containing promoters[16]. Type II IFN-γ causes gene activation of gamma activated sequence (GAS) containing promoters. Pro-inflammatory cytokine signalling (TNFα and IL-1α) induces genes containing NF-κB sites in the promoter. Signalling of type I IFNs (IFN-α and IFN-β), type II IFN (IFN-γ), type III IFN (IFN-λ1) and pro-inflammatory cytokine signalling (TNFα and IL-1α) was quantified using quantitative Firefly luciferase reporters controlled by the respective promoters (Fig. 1c). Stimulation with IFN-α2 and IFN-β (Fig. 1c) revealed that activation of the ISRE promoter is strongly repressed by Nsp1, Nsp5, Nsp13, Nsp14, ORF6 and ORF7b. A similar set of viral proteins interfered with type II IFN-γ and type III IFN-λ1 signalling, albeit much weaker (mean inhibition 18% and 35%, respectively) compared to type I IFN signalling (mean inhibition 78% for IFN-α2 and 53% for IFN-β). Activation of NF-κB signalling by TNFα or IL-1α was potently inhibited by the SARS-CoV-2 Nsp1, Nsp5, Nsp15, ORF3a, E, M, ORF6 and ORF7b proteins. These analyses revealed that a similar set of proteins (Nsp1, Nsp5, Nsp15, ORF3a, E, M, ORF6 and ORF7b) antagonises pro-inflammatory cytokine induction and signalling.

Since induction of autophagy does not depend on *de novo* gene expression[41], we monitored autophagy levels in SARS-CoV-2 protein expressing HEK293T cells by membrane-association of stably expressed GFP-LC3B, a hallmark of autophagy induction (Fig. 1d, Supplementary Fig. 1e)[42]. Autophagosome numbers under basal conditions were strongly increased in the presence of ORF3a, E, M and ORF7a, suggesting either *de novo* induction of autophagy or blockage of turnover (Fig. 1d). Upon induction of autophagy using Rapamycin, a similar pattern was observed. To clarify whether these viral proteins induce autophagy or block turnover, leading to accumulation of GFP-LC3B positive vesicles, we treated cells with saturating amounts of Bafilomycin A1, which inhibits autophagic turnover. The increase of autophagosome numbers by ORF3a, E, M and ORF7a was drastically reduced compared to non-blocking conditions (Fig. 1d), indicating that these proteins block turnover, rather than induce it. Blockage of autophagy and co-expression of Nsp1 and Nsp14 induced cell death, which may be

bioRxiv preprint doi: https://doi.org/10.1101/2020.10.15.340612; this version posted October 15, 2020. The copyright holder for this preprint (which was not certified by peer review) is the author/funder, who has granted bioRxiv a license to display the preprint in perpetuity. It is made available under aCC-BY-NC-ND 4.0 International license.

151 responsible for the low number of autophagosomes. Unexpectedly, in the presence of Nsp15
152 autophagosome numbers were consistently reduced, suggesting that it inhibits autophagy (Fig. 1d).

153 Taken together, our analysis reveals that SARS-CoV-2 encodes multiple proteins that strongly
154 antagonise innate immunity. Notably, there are differences in overall inhibition of the pathways with
155 IFN-γ and IFN-λ1 signalling being only weakly antagonised. Furthermore, autophagy turnover is
156 strongly blocked by E, M, ORF3a and ORF7a, thus autophagic degradation is avoided.

157 **SARS-CoV-2 proteins target innate immunity at multiple levels**

158 Our analyses revealed that IFN-β signalling as well as autophagy are strongly counteracted by multiple
159 SARS-CoV-2 proteins. Therefore, we aimed at identifying the steps that are targeted in these pathways.
160 We focused on the top 5 inhibitors as identified in Fig. 1b-d. Nsp1 was removed from the analysis as it
161 prevents translation in general[30]. To analyse IFN-β signalling, we monitored the levels of the type I IFN
162 receptor, IFNAR using western blotting in HEK293T cells overexpressing Nsp5, Nsp13, Nsp14, ORF6
163 or ORF7b. Activation of the two major transcription factors of type I IFN signalling, STAT1 and
164 STAT2 (Fig. 2a), was examined by phosphorylation status. Basal STAT1 and STAT2 levels were not
165 significantly affected by all proteins tested (Fig. 2b, quantification in Supplementary Fig. 2a-c). (Fig.
166 2b). In the presence of Nsp5, activated STAT1 and to a lesser extent STAT2 accumulated (Fig. 2b and
167 2d, Supplementary Fig. 2a). ORF6 and ORF7b neither affect IFNAR levels nor STAT1 expression nor
168 activation (Fig. 2b-d). This agrees with recent reports[26,43,44] suggesting that ORF6 instead prevents
169 trafficking of transcription factors. In the presence of Nsp14 and to a lesser extent Nsp13, endogenous
170 levels of IFNAR were prominently reduced (Fig. 2b, c). Consequently, phosphorylation of STAT1 was
171 decreased upon Nsp14 co-expression (Fig. 2b, d).

172 Upon activation of autophagy, cytoplasmic MAP1LC3B (LC3B) is proteolytically processed and
173 lipidated (LC3B-II) to decorate autophagosomal membranes[41,42]. Upon fusion of autophagosomes with
174 lysosomes, the autophagic receptor p62 is degraded (autophagy turnover, Fig. 2e). We analysed the
175 effect of the top 5 autophagy modulating SARS-CoV-2 proteins: Nsp15, ORF3a, E, M and ORF7a (Fig.
176 1d) on autophagy markers. Levels of Beclin-1 and ULK1, which are part of the core machinery of

bioRxiv preprint doi: https://doi.org/10.1101/2020.10.15.340612; this version posted October 15, 2020. The copyright holder for this preprint (which was not certified by peer review) is the author/funder, who has granted bioRxiv a license to display the preprint in perpetuity. It is made available under aCC-BY-NC-ND 4.0 International license.

autophagy initiation[45,46], remained constant (Fig. 2f, Supplementary Fig. 2d and 2e). Overexpression of Nsp15 led to a very slight decrease of LC3B-II but accumulation of p62, suggesting that Nsp15 blocks induction of autophagy (Fig. 2f and 2g-h). In line with this, the number of GFP-LC3B-puncta (=autophagosomes) per cell in HeLa-GFP-LC3B cells was reduced upon Nsp15 expression to almost 0 (Fig. 2i, j). In the presence of ORF3a, E and ORF7a, the levels of processed LC3B (LC3B-II) were 4- to 7-fold increased (Fig. 2g), and p62 levels were approximately 1.5-fold increased (Fig. 2h). This indicates that these three viral proteins block autophagic turnover. Consequently, the number of autophagosomes was 10-fold increased upon ORF3a, E, M or ORF7a expression (Fig. 2i, j). Curiously, while accumulation of LC3B-II indicated that M blocks autophagic turnover or induces autophagy, the levels of p62 were not significantly altered in the presence of M (Fig. 2f, h). Notably, overexpression of M resulted in an accumulation of LC3B in the perinuclear space, whereas for all other viral proteins autophagosomes were normally distributed (Fig. 2i, j).

Taken together, our data demonstrates that SARS-CoV-2 synergistically targets innate immune activation. The major type I IFN antagonists Nsp5, Nsp13, Nsp14, ORF6 and ORF7b block the signalling cascade at different levels. E, ORF3a and ORF7a use similar mechanism to block autophagic turnover, while M may have evolved a different mechanism and Nsp15 inhibits *de novo* autophagy induction.

ORF3a and ORF7a perturb the late-endosomal/trans-Golgi network

Our data showed that ORF3a and ORF7a are potent autophagy antagonists of SARS-CoV-2 (Fig. 1d, Fig. 2f-j). To determine their molecular mechanism(s), we performed proteome analysis of HEK293T cells overexpressing SARS-CoV-2 ORF3a and ORF7a (Supplementary Fig. 3a). As a control, we used S, Nsp1 and Nsp16 overexpressing cells which show little to no effect on autophagy (Fig. 1d). In addition, we analysed the proteome of Caco-2 cells infected with SARS-CoV-2 for 24 or 48 h. Fold changes compared to vector transfected or non-infected controls were calculated (Fig. 3a, b, Supplementary Fig. 3b-e, Supplementary Table 1). Analysis of the data revealed that in the presence of Nsp1, cellular proteins with a short half-life were markedly reduced (Supplementary Fig. 3f)[47]. This supports our previous finding that Nsp1 globally blocks translation[30] and confirms the validity of the

bioRxiv preprint doi: https://doi.org/10.1101/2020.10.15.340612; this version posted October 15, 2020. The copyright holder for this preprint (which was not certified by peer review) is the author/funder, who has granted bioRxiv a license to display the preprint in perpetuity. It is made available under aCC-BY-NC-ND 4.0 International license.

proteome analysis. PANTHER-assisted Gene Ontology Analysis of the proteins regulated more than 4-fold by the overexpression of individual SARS-CoV-2 proteins revealed that ORF3a and ORF7a target the late endosome pathway (GO:0005770) (Fig. 3c, Supplementary Table 2). A similar analysis for the SARS-CoV-2 samples showed that the late endosome pathway is also affected during the genuine infection. Thus, we had a closer look at the subcellular localisation of ORF3a and ORF7a and their effect on intracellular vesicles. In line with the proteome analysis, ORF7a and ORF3a both localised to the late endosomal compartment, co-localising with the marker Rab9 (Fig. 3d, e). In contrast, localisation to Rab5a-positive early endosomes was not apparent (Supplementary Fig. 3g). Disturbance of the integrity of the trans-Golgi network (TGN) at the interface with the late endosomes[48,49] by viral proteins is a well-known strategy to block autophagy[50]. Immunofluorescence analysis revealed that the localisation of ORF3a or ORF7a partially overlapped with a TGN marker (R = 0.5, Fig. 3g) indicating close proximity. ORF6, which is known to localise to the Golgi apparatus[43], was used a positive control (R=0.7). Nsp8, which displayed a cytoplasmic localisation, was used as a negative control (R=0.3). Importantly, analysis of free TGN-marker positive vesicles in SARS-CoV-2 ORF3a or ORF7a expressing cells revealed that both viral proteins cause significant fragmentation of the TGN (Fig. 3f, h).

These data indicate that both ORF3a and ORF7a disturb the proteome at the late endosomes eventually causing the TGN to fragment, which ultimately leads to a block of autophagic turnover[49–52].

SARS-CoV-2 Nsp15 is less potent in innate immune antagonism than SARS-CoV-1 Nsp15

To examine the conservation of innate immune antagonism, we functionally compared Nsp1, Nsp3, Nsp7, Nsp15, M, N, ORF3a, ORF6 and ORF7a of SARS-CoV-2, the closest related CoV, RaTG13-CoV and the previous highly pathogenic SARS-CoV-1. RaTG13-CoV was isolated from the intermediate host horseshoe bats (*Rhinolophus affinis*)[3]. The amino acid sequences of the different CoVs are largely conserved, with the exception of Nsp3, ORF3a and ORF6 (Fig. 4a), and were all expressed as confirmed by western blotting (Supplementary Fig. 4a-i). Rabies virus P protein[53–55], Measles virus V protein[56–58] and TRIM32[59,60] expression served as positive controls. Overall, proteins of SARS-CoV-1 and RaTG13-CoV behave similar to their SARS-CoV-2 counterparts, suggesting that

bioRxiv preprint doi: https://doi.org/10.1101/2020.10.15.340612; this version posted October 15, 2020. The copyright holder for this preprint (which was not certified by peer review) is the author/funder, who has granted bioRxiv a license to display the preprint in perpetuity. It is made available under aCC-BY-NC-ND 4.0 International license.

many functions are conserved. Importantly, however, this is not the case for Nsp15, Nsp3 and to a lesser extend ORF6 (Fig. 4a-c). SARS-CoV-1 ORF6 is about 4-fold less potent in antagonising type I IFN signalling (Fig. 4b) but induces higher levels of autophagy (Fig. 4c). However, expression levels of SARS-CoV-1 ORF6 were also higher than that of its SARS-CoV-2 and RaTG13-CoV counterparts (Supplementary Fig. 4g), which may explain the differences in activity. Significant differences between SARS-CoV, RaTG13-CoV and SARS-CoV-2 Nsp3 were reanalysed in a dose-dependent manner, however the differences are only in the range of 2-3-fold (Supplementary Fig. 4j).

The most striking, statistically significant difference was observed for Nsp15. SARS-CoV-1 Nsp15 is over 10-fold more potent in suppression of type I IFN induction and signalling than RaTG13-CoV and SARS-CoV-1 Nsp15 (Fig. 4a, b). Notably, expression levels of SARS-CoV-2, RaTG13-CoV and SARS-CoV-1 Nsp15 were similar, with SARS-CoV-1 Nsp15 even slightly less expressed (Supplementary Fig. 4c). Notably, all Nsp15 variants still inhibited autophagy equally (Fig. 4c). Analysis of the dose-dependent effect of SARS-CoV-2 Nsp15, RaTG13-CoV Nsp15 and SARS-CoV-1 Nsp15 on type I IFN induction (Fig. 4d) and signalling (Fig. 4e) showed that on average SARS-CoV-2 Nsp15 performed 32-fold worse than SARS-CoV-1 Nsp15, and RaTG13-CoV Nsp15 inhibited type I IFN induction 7.8-fold less (Fig. 4d). Similarly, SARS-CoV-1 Nsp15 outperformed RaTG13-CoV and SARS-CoV-2 Nsp15 by 15- and 5.7-fold, respectively, in inhibition of type I IFN signalling (Fig. 4e).

Taken together, this data indicates, that while most IFN antagonist activities are conserved between SARS-CoV-1, RaTG13-CoV and SARS-CoV-2, there is a major exception: Nsp15 of SARS-CoV-2 was considerably less potent than SARS-CoV-1 Nsp15 in counteracting both IFN-β induction and signalling.

Inefficient antagonism by SARS-CoV-2 proteins is predictive for efficient immune control

Our analyses revealed that several of the 29 SARS-CoV-2 proteins synergistically antagonise innate immune activation (Figs. 1-4), albeit with different efficiency. The mean inhibition of IFN-γ and IFN-λ1 signalling was only 18% and 35%, respectively, compared to type I IFN signalling with a mean inhibition of 78% for IFN-α2 and 53% for IFN-β. Consequently, we assessed whether IFN-α2, IFN-β,

bioRxiv preprint doi: https://doi.org/10.1101/2020.10.15.340612; this version posted October 15, 2020. The copyright holder for this preprint (which was not certified by peer review) is the author/funder, who has granted bioRxiv a license to display the preprint in perpetuity. It is made available under aCC-BY-NC-ND 4.0 International license.

IFN-γ and IFN-λ1 have a different impact on SARS-CoV-2 (Fig. 5a, Supplementary Fig. 5a, b). Treatment with the type I IFN-α2 was the least efficient. In contrast, at the same concentration IFN-γ (500 U/ml) reduced viral RNA in the supernatant almost 300-fold more efficiently. All agents caused little if any cytotoxic effects (Supplementary Fig. 5c). Altogether, we observed a good correlation (r= 0.89) between average inhibition of the respective signalling pathway (Fig. 1c) antagonised by the 29 SARS-CoV-2 proteins and IFN susceptibility at 5 U/ml (Fig. 5b). Thus, our results indicate that the overall efficiency of SARS-CoV-2 proteins in counteracting specific IFN signalling pathway is predictive for the overall antiviral potency of different types of IFNs.

Rational combination allows highly effective innate control of SARS-CoV-2

IFN therapy is commonly associated with significant adverse effects, due to inflammation. To minimize detrimental pro-inflammatory effects of IFNs, doses required for efficient viral restriction should be reduced. Thus, we analysed the impact of the most potent IFNs, IFN-γ and IFN-λ1, and their combination on SARS-CoV-2 replication. To mimic prophylactic and therapeutic treatment, we examined pre-treatment for 24 h before infection with SARS-CoV-2 and treatment 6 h post-infection. Overall, the effects of IFN treatment were about 10-fold stronger in the prophylactic condition than in the therapeutic treatment but consistent (Fig. 5c, d). Expression analysis of SARS-CoV-2 S and N confirmed the qPCR results, and equal GAPDH levels show no cytotoxicity (Fig. 5d). While treatment with a single dose of IFN-γ and IFN-λ1 alone reduced viral RNA production 50-100-fold, the combinatorial treatment at the same concentration synergistically potentiated the effect to about 1000-fold reduction in SARS-CoV-2 RNA (Fig. 5c).

To further decrease inflammatory side-effects by IFN treatment, anti-inflammatory pathways like autophagy could be induced[61–63]. Treatment with Rapamycin, which induces autophagy, already reduced viral replication to a maximum of 4-6-fold on its own at 125 nM (Supplementary Fig. 5d, e). Bafilomycin A1, which blocks autophagy, had little to no effects. Both drugs only marginally affected cell survival at the used concentrations (Supplementary Fig. 5f). Treatment of Rapamycin (125 nM) in combination with either IFN-γ or IFN-λ1 was found to be additive (Fig. 5c, d). Triple treatment with IFN-γ, IFN-λ1 and Rapamycin showed the most potent anti-viral effect of all combinations for pre-

bioRxiv preprint doi: https://doi.org/10.1101/2020.10.15.340612; this version posted October 15, 2020. The copyright holder for this preprint (which was not certified by peer review) is the author/funder, who has granted bioRxiv a license to display the preprint in perpetuity. It is made available under aCC-BY-NC-ND 4.0 International license.

284 treatment and post-treatment, reducing viral RNA in the supernatant by ~2100-fold and ~86-fold,
285 respectively (Fig. 5c).

286 In summary, our data shows that the anti-SARS-CoV-2 effect of combinatorial treatments of IFN-γ,
287 IFN-λ1 are synergistic. Additional anti-inflammatory autophagy activation by Rapamycin even further
288 decreased SARS-CoV-2 replication. This suggests that concerted activation of innate immunity may be
289 an effective anti-viral approach ensuring low inflammation.

290 **DISCUSSION**

291 Viruses drastically alter our innate immune defences to establish an infection and propagate to the next
292 host[13,14,21,27,43,64]. Our data reveal the extent of immune manipulation SARS-CoV-2 employs. We
293 determined the major antagonists of type I, type II and type III IFN induction and signalling as well as
294 pro-inflammatory NF-κB activity encoded by SARS-CoV-2 (Nsp1, Nsp5, Nsp13, Nsp14, ORF6 and
295 ORF7b). In addition, autophagy is majorly targeted by Nsp15, ORF3a, E, M and ORF7a. Subsequent
296 mechanistic studies revealed that SARS-CoV-2 proteins synergistically block innate immune induction
297 at various levels. We could reveal for the first time, that Nsp14 lowers the cellular levels of the IFN
298 receptor, IFNAR, consequently preventing activation of the crucial transcription factors STAT1 and
299 STAT2. Both ORF3a and ORF7a cause fragmentation of the TGN via disturbing the late endosomal
300 pathway. This is a common strategy of viruses to block autophagic turnover[50]. Examination of the
301 functional conservation showed that SARS-CoV-2 Nsp15 was less efficient in blocking innate immune
302 activation, both type I IFN induction and signalling, than SARS-CoV-1 Nsp15. This may ultimately
303 cause SARS-CoV-2 to be better controlled by the innate immune system than SARS-CoV, impacting
304 the number of subclinical infections and eventually facilitate efficient spread. Thus, our data suggests
305 that differences in innate immune antagonism by Nsp15 could have contributed to the rapid spread of
306 SARS-CoV-2. Overall, the combined analysis of IFN antagonism allowed us to deduce that treatment
307 with IFN-γ and IFN-λ1 is most efficient against SARS-CoV-2. On top of that, combinatorial treatment
308 of SARS-CoV-2 with these two IFNs and anti-inflammatory autophagy induction potentiated the effects
309 of the individual treatments. This may pave the way for future anti-viral therapies against SARS-CoV-
310 2 based on rational immune activation.

bioRxiv preprint doi: https://doi.org/10.1101/2020.10.15.340612; this version posted October 15, 2020. The copyright holder for this preprint (which was not certified by peer review) is the author/funder, who has granted bioRxiv a license to display the preprint in perpetuity. It is made available under aCC-BY-NC-ND 4.0 International license.

Why would multiple effective proteins target the same pathway? For example, type I IFN signalling could have been shut down by Nsp1, Nsp5, Nsp13, Nsp14, ORF6 and ORF7b alone, each reducing the activation of the innate immune pathways to below 10%. However, our assays revealed (Figs. 1-3) that the targeting mechanisms are often not redundant and may act synergistically. This could allow the virus to better control the targeted pathway, thus minimising the effect of the signalling on its replication. In addition, a viral protein majorly targeting one pathway may affect other connected immune pathways at once. For example, disturbance of the kinase TBK1 activation may affect primarily IFN induction and to a lesser extend also impact autophagy[65]. Proteome analyses revealed the late endosome/Golgi network as a target of ORF3a and ORF7a. Our data suggests, that both ORF3a and ORF7a of SARS-CoV-2 cause fragmentation of the Golgi apparatus and thus likely blockage of autophagy. SARS-CoV-1 ORF3a was previously implicated in Golgi fragmentation[51,66]. Notably, fragmentation of the Golgi is for example triggered by Hepatitis C virus to block anti-viral autophagic turnover[50] and may represent a common strategy by viruses to avoid autophagic degradation. Based on our initial proteome approaches, future studies will see more mechanistic data to explain the molecular details of the impact of SARS-CoV-2 proteins on innate immune activation. Notably, several proteins including ORF6, ORF3a, ORF7a, M and E, accumulate at the Golgi network or in perinuclear spaces, alluding to the emerging role of the Golgi as a hub for immune manipulation[52,67].

Our results demonstrate that ORF6, ORF3a, ORF7a and ORF7b are the strongest innate immune antagonists among the accessory genes of SARS-CoV-2 (Fig. 1). Besides the accessory genes, which classically encode immune antagonists, a surprising number of non-structural proteins manipulate innate immunity. Nsp1, which targets cellular translation and thus broadly inhibits any response dependent on cellular translation, including IFN induction and expression of ISGs[30]. However, Nsp3, Nsp5, Nsp13 and to a lower extend Nsp15 also antagonised IFN induction and signalling (Fig. 1). These non-structural proteins of CoVs have important functions in the viral life-cycle: Nsp3 as ISG/ubiquitin ligase and protease for autocatalytic processing of the ORF1a/b precursor protein[68–70] Nsp5 as a protease mediating cleavage of the precursor polyproteins[71,72], Nsp13 as NTPase/Helicase[73,74] and Nsp15 as endoribonuclease[75]. So far it is not completely clear how their enzymatic functions may impact their

bioRxiv preprint doi: https://doi.org/10.1101/2020.10.15.340612; this version posted October 15, 2020. The copyright holder for this preprint (which was not certified by peer review) is the author/funder, who has granted bioRxiv a license to display the preprint in perpetuity. It is made available under aCC-BY-NC-ND 4.0 International license.

activity against innate immunity. Except for Nsp3, as its function as a de-ISGlase may inactivate the transcription factor IRF3 and thus reduce IFN induction[70]. According to our analysis the structural proteins E and M strongly manipulated autophagy (Fig. 1d). This suggests that the incoming virion may already block autophagic turnover to prevent their own degradation by autophagy.

However, while we may detect most counteraction strategies, our screening approach may miss immune evasion strategies employed by SARS-CoV-2. For example, many non-structural proteins form complexes, that are not preent during single overexpression and may only be functional as a full assembly. Evasion mechanisms based on RNA structures and sequences will not be identified due to the usage of codon-optimized expression plasmids. Finally, the virus itself may employ strategies to hide itself from recognition, not activating innate immune defences in the first place. One example is the capping of its genomic and subgenomic mRNAs, which removes the free triphosphate 5'end.

Our analyses further revealed that the human innate immune antagonism is largely conserved in an animal CoV isolate that is sequentially closest related to SARS-CoV-2, RaTG13-CoV[1,76] (Fig. 4). This indicates that the virus from horseshoe bats is capable of counteracting the human immune defences, which may have facilitated successful zoonotic transmission from bats eventually to humans. Currently, the intermediate animal host of SARS-CoV-2 is under debate[3,76–78], however it is likely, that the virus isolated from it is even closer related to SARS-CoV-2 than RATG13-CoV. Thus, any immune evasion mechanisms conserved between SARS-CoV-2 and RATG13-CoV, is likely to be conserved in the direct progenitor virus of SARS-CoV-2. The previous epidemic and related human SARS-CoV-1 and the current pandemic SARS-CoV-2 differ in susceptibility towards IFNs with SARS-CoV-1 being more resistant[26]. Furthermore, infection with SARS-CoV-2 is often asymptomatic and likely controlled by the host[26] as lower mortality rates and higher subclinical infections suggest[4]. Paradoxically, this may support the fast spread and 'success' of the virus. Thus, SARS-CoV-2 may have found the 'perfect' balance. Intermediate immune evasion and consequently intermediate pathogenicity to support spread, but not kill the host. Our data shows that SARS-CoV-2 Nsp15 is strikingly less in efficient in IFN evasion than Nsp15 of SARS-CoV. These data are the first mechanistic evidence why SARS-CoV-1 is

bioRxiv preprint doi: https://doi.org/10.1101/2020.10.15.340612; this version posted October 15, 2020. The copyright holder for this preprint (which was not certified by peer review) is the author/funder, who has granted bioRxiv a license to display the preprint in perpetuity. It is made available under aCC-BY-NC-ND 4.0 International license.

less susceptible towards IFN treatment than SARS-CoV-2. It may be tempting to speculate that common cold CoVs counteract the innate immune system less efficiently than SARS-CoV-2.

Our analysis indicates that during a SARS-CoV-2 infection less cytokines than expected are released, autophagic turnover is blocked and general immune activation is perturbed. This is supported by a large amount of data from COVID19 patients[24–28,43,70,79–81]. However, an important question remains: Why are some innate immune pathways, such as IFN-γ signalling less antagonised (Fig. 1)? Are the viral immune manipulation strategies ineffective? Indeed, IFN-γ is the most potent IFN against SARS-CoV-2 we and others tested[80] (Fig. 5). One possible explanation would be that there was no need for the virus to antagonise them. Indeed, in COVID19 patients and in vitro infections with SARS-CoV-2, IFN-γ levels are surprisingly low[28,81]. Furthermore, despite high IFN-γ levels being a hallmark of cytokine storms induced by influenza viruses, the SARS-CoV-2 cytokine storm only has low IFN-γ levels and decreased IFN-γ expression in CD4+ T cells is associated with severe COVID19[4,82,83]. It is tempting to speculate that T-cells which confer pre-existing immunity against SARS-CoV-2[84,85] could, upon activation, release IFN-γ, whose innate immune signalling may also contribute to increased clearance of the infection. Strikingly, our work shows that analysis of the innate antagonism may be predictive for therapeutic opportunities.

Severe side effects due to high and constant inflammation are prevalent for treatments with IFNs[35–37]. However, theses side-effects are dose-dependent[86]. Thus, minimizing the dose required for treatment is paramount. Our data indicates that effects of treatment with multiple IFNs is additive but synergistic and potentiates each other (Fig. 5). Therefore, a promising anti-viral approach may be a combinatorial treatment of different cytokines, effectively also reducing the burden of side-effects. The side effects of IFN therapy are mainly caused by inflammation. Combined with anti-inflammatory approaches such as autophagy activation by Rapamycin[62,63], this approach may even be more successful, as our *in vitro* data suggests. Future studies are highly warranted to study rational, concerted innate immune activation against SARS-CoV-2 *in vivo*. These studies may eventually pave the way for novel therapies, which may not only work against SARS-CoV-2, but also against other pathogenic viruses, including potentially future CoVs.

bioRxiv preprint doi: https://doi.org/10.1101/2020.10.15.340612; this version posted October 15, 2020. The copyright holder for this preprint (which was not certified by peer review) is the author/funder, who has granted bioRxiv a license to display the preprint in perpetuity. It is made available under aCC-BY-NC-ND 4.0 International license.

391 In summary, our results reveal the extend of innate immune manipulation of SARS-CoV-2. The
392 comparison of innate antagonism of SARS-CoV-2 to SARS-CoV-1 revealed that mutations in Nsp15
393 may be responsible for the higher susceptibility of SARS-CoV-2 against IFNs. Finally, our data allowed
394 us to deduce the most effective IFNs against SARS-CoV-2 and combinatorial treatments even further
395 minimized the doses of the individual cytokines required.

396

397 **AUTHOR CONTRIBUTIONS**

398 L.K., M.Hi., M.Ha. performed the majority of the experimental work with help from J.H.S.,
399 S.K. and C.B.P.. R.N. performed experiments with infectious SARS-CoV-2 assisted by F.Z..
400 C.M.S. and S.S. generated expression constructs. J.A.M. and C.C. performed the SARS-CoV-
401 2 infection for the proteome analysis. A.I., I.F. and W.A performed the proteome analyses and
402 the bioinformatic interrogation of the data. J. M., D.S., A.I., S.S. and K-K.C. provided
403 resources and comments for the manuscript. K.M.J.S and F.K. conceived the study, planned
404 experiments and wrote the manuscript. All authors reviewed and approved the manuscript.

405

406 **ACKNOWLEDGEMENTS**

407 We thank Regina Burger, Susanne Engelhart, Daniela Krnavek, Kerstin Regensburger, Martha
408 Meyer, Birgit Ott and Nicola Schrott for excellent technical assistance. We would like to
409 especially acknowledge the library of SARS-CoV-2 expression plasmids which was
410 generously given to us by Nevan Krogan (University of California, San Francisco). This study
411 was supported by DFG grants to F.K., J.M., K.M.J.S., D.Sa., A.I. and KKC (CRC1279,
412 SPP1923, SP1600/4-1, CRC1309, Project-ID 369799452 - TRR237), EU's Horizon 2020
413 research and innovation program to J.M. (Fight-nCoV, 101003555), a COVID-19 research
414 grant of the Federal Ministry of Education and Research (MWK) Baden-Württemberg (to D.S.

bioRxiv preprint doi: https://doi.org/10.1101/2020.10.15.340612; this version posted October 15, 2020. The copyright holder for this preprint (which was not certified by peer review) is the author/funder, who has granted bioRxiv a license to display the preprint in perpetuity. It is made available under aCC-BY-NC-ND 4.0 International license.

and F.K.) as well as the BMBF to F.K., D.Sa. and K.M.J.S. (Restrict SARS-CoV-2, protACT and IMMUNOMOD).

DECLARATIONS OF INTERESTS

The authors declare no competing interests.

FIGURE LEGENDS

Figure 1: Systematic analysis of innate immune antagonism by SARS-CoV-2 proteins. a, Schematic depiction of the 30 SARS-CoV-2 encoded proteins in the order they appear in the genome. The polyprotein ORF1a(b) is (auto)proteolytically cleaved into 16 non-structural proteins (Nsp, turquoise). The structural proteins (yellow) are Spike (S), Membrane (M), envelope (E) and nucleoprotein (N). The set is complemented by the accessory proteins (red) ORF 3a, 3b, 3c, 6, 7a, 7b, 8, 9b, 9c and 10. **b-d**, Schematic depiction of the assay setup (top panel) and heatmap (red = inhibition, blue = induction) depicting modulation of innate immune pathways by overexpression of indicated SARS-CoV-2 proteins. Stimuli of the immune pathways are indicated. (a, b) Readout by luciferase reporter gene assay (colour represents the mean of n=3) using indicated promoter constructs in HEK293T cells or (c) autophagosome measurement by quantification of membrane-associated GFP-LC3B in HEK293T-GFP-LC3B cells (colour represents the mean of n=4). The stimulated vector control is set to 100% (white). SeV, Sendai Virus. IFN, Interferon. NT, not treatment. Rapa, Rapamycin. BafA, Bafilomycin A1.

Figure 2: SARS-CoV-2 interferes with innate immunity at various levels. a, Schematic depiction of the type I IFN signalling pathway. **b**, Exemplary immunoblot analysis showing activation of type I IFN signalling markers using whole cell lysates (WCLs) of HEK293T cells expressing indicated proteins and stimulated with IFN-β (1000 U/ml, 45 min). Blots were

bioRxiv preprint doi: https://doi.org/10.1101/2020.10.15.340612; this version posted October 15, 2020. The copyright holder for this preprint (which was not certified by peer review) is the author/funder, who has granted bioRxiv a license to display the preprint in perpetuity. It is made available under aCC-BY-NC-ND 4.0 International license.

stained with anti-pSTAT1, anti-STAT1, anti-pSTAT2, anti-STAT2, anti-IFNAR, anti-Strep II and anti-actin. **c**, Quantification of the band intensities in (b) for IFNAR normalized to the band intensities of actin. Bars represent mean of n=3±SEM. **d**, Quantification of the band intensities in (b) for phospho-STAT1 (pSTAT1) normalized to the band intensities of actin. Bars represent mean of n=3±SEM. **e**, Schematic depiction of autophagy. **f**, Exemplary immunoblot analysis showing autophagy activity markers using WCLs of HEK293T cells expressing indicated proteins. Blots were stained with anti-SQSTM1/p62, anti-LC3B-II, anti-Beclin-1, anti-ULK1, anti-Strep II and anti-actin. **g**, Quantification of the band intensities in (f) for LC3B-II normalized to the band intensities of actin. Bars represent mean of n=3±SEM. **h**, Quantification of the band intensities in (f) for p62 normalized to the band intensities of actin. Bars represent mean of n=3±SEM. **i**, Exemplary confocal laser scanning microscopy images of autophagy activation via GFP-LC3B (green) puncta formation. Indicated Strep II-tagged SARS-CoV-2 proteins (red) were overexpressed in HeLa GFP-LC3B cells (green). CQ, Chloroquine (4 h 10 µM) was used as a positive control. Nuclei, DAPI (blue). Scale bar, 25 µM. **j**, Quantification by area of GFP-LC3B puncta divided by cell number from the images in (i). Bars represent the mean of n=38-100 cells±SEM.

Figure 3: ORF3a and ORF7a disturb the trans-Golgi network/late endosome interface. **a**, Heatmap (red = downregulation, blue = upregulation) depicting the fold changes of cellular and viral proteins during overexpression of indicated single SARS-CoV-2 proteins in HEK293T cells or **b**, SARS-CoV-2 infection (MOI 1) of Caco-2 cells 24 or 48 h post infection as assessed by mass spectrometry. **c**, Scatter plots of log2 fold enrichment and P-value of the GO-Term ‘late endosome’ in protein sets regulated more than 4-fold upon expression of indicated viral protein (a) or SARS-CoV-2 infection (b). **d**, Quantification of co-localisation by Pearson Correlation of Rab9 and indicated viral proteins in HeLa cells transiently transfected with the indicated viral protein and GFP-Rab9. Bars represent the mean of n=7-15

bioRxiv preprint doi: https://doi.org/10.1101/2020.10.15.340612; this version posted October 15, 2020. The copyright holder for this preprint (which was not certified by peer review) is the author/funder, who has granted bioRxiv a license to display the preprint in perpetuity. It is made available under aCC-BY-NC-ND 4.0 International license.

cells±SEM. **e**, Exemplary confocal microscopy images of HeLa cells transiently expressing indicated viral proteins (red) and a marker of late endosomes GFP-Rab9 (green). Cells were stained with anti-Strep II (red). Nuclei, DAPI (blue). Scale bar, 10 µm. **f**, Exemplary confocal microscopy images of the quantification in (g) stained with anti-TGN46 (green) and anti-Strep II (red). Nuclei, DAPI (blue). Scale bar, 10 µm. **g**, Pearson's correlation indicating co-localisation between TGN46 and the indicated viral proteins from the image in (f). Bars represent the mean of n=6 cells±SEM. **h**, Quantification of non-Golgi associated vesicles per cell as puncta/cell of (f). Bars represent the mean of n=15-25 cells ±SEM.

Figure 4: Conservation of innate immune antagonism between SARS-CoV-2, RaTG13-CoV and SARS-CoV. **a-c**, Immune activation of type I IFN induction (a), type I IFN signalling (b) or autophagy (c) in the presence of indicated proteins (Nsp1, Nsp3, Nsp7, Ndsp15, M, N, ORF3a, ORF6, ORF7a) of SARS-CoV-2 (blue), RaTG13-CoV (purple) or SARS-CoV-1 (red) assessed by IFN-β-promoter luciferase reporter gene assays stimulated with Sendai Virus (SeV, a). ISRE-promoter luciferase reporter gene assays stimulated with IFN-β (1000 U/ml, b). Membrane-associated GFP-LC3B (c) (n=4±SEM). Vector induction set to 100% (black). Controls, RABV P, MeV V or TRIM32 (grey). Bars represent the mean of n=3±SEM (a,b) or n=4±SEM (c). **d**, Dose dependent effect of SARS-CoV-2, RaTG13-CoV or SARS-CoV-1 Nsp15 expression on IFN-β induction stimulated with SeV (24 h). Quantification by IFN-β promoter dependent luciferase reporter activity. Lines represent one individual replicate. **e**, Dose dependent effect of Nsp15 expression on IFN-β signalling in HEK293T cells, stimulated with IFN-β (1000 U/ml, 8 h). Quantification by ISRE promoter dependent luciferase reporter activity. Lines represent one individual replicate.

Figure 5: Innate immune activation as an anti-viral approach. a, SARS-CoV-2 N RNA in the supernatant of SARS-CoV-2 (MOI 0.05, 48h p.i.) infected Calu-3 cells that were left untreated and/or were treated with the indicated amounts of indicated IFNs or pro-

bioRxiv preprint doi: https://doi.org/10.1101/2020.10.15.340612; this version posted October 15, 2020. The copyright holder for this preprint (which was not certified by peer review) is the author/funder, who has granted bioRxiv a license to display the preprint in perpetuity. It is made available under aCC-BY-NC-ND 4.0 International license.

inflammatory cytokines as assessed by qPCR. Lines represent the mean of n=2±SD. **b**, Correlation between average inhibition of the indicated innate immune signalling pathway and impact on replication of SARS-CoV-2 after treatment with the respective cytokine. r, Pearson's correlation. **c**, SARS-CoV-2 N RNA in the supernatant of SARS-CoV-2 (MOI 0.05, 48h p.i.) infected Calu-3 cells that were left untreated and/or were treated with the indicated combinations of indicated IFNs (5 U/ml) or Rapamycin (125 nM) either 24 h before the infection (Pre-treatment) or 6 h post infection (Post-treatment). Dots represent individual experiments, line the mean. Fold reduction compared to control is indicated. **d**, Immunoblot analysis of the SARS-CoV-2 infection using the WCLs of Calu-3 cells in (c). Blots were stained with anti-SARS-CoV-2 S, anti-SARS-CoV-2 N, and anti-GAPDH.

MATERIAL AND METHODS

Cell lines and cell culture and viruses. HEK293T cells were purchased from American type culture collection (ATCC: #CRL3216). The construction of HEK293T GL cells and HeLa GL cells was reported previously[42]. These cell lines were cultivated in Dulbecco's Modified Eagle Medium (DMEM, Gibco) supplemented with 10% (v/v) fetal bovine serum (FBS, Gibco), 100 U/ml penicillin (PAN-Biotech), 100 µg/ml Streptomycin (PAN-Biotech), and 2 mM L-glutamine (PANBiotech). Calu-3 (human epithelial lung adenocarcinoma, kindly provided and verified by Prof. Frick, Ulm University) cells were cultured in Minimum Essential Medium Eagle (MEM, Sigma) supplemented with 10% (v/v) FBS (Gibco) (during viral infection) or 20% (v/v) FBS (Gibco) (during all other times), 100 U/ml penicillin (PAN-Biotech), 100 µg/ml Streptomycin (PAN-Biotech), 1 mM sodium pyruvate (Gibco), and 1x non-essential amino acids (Gibco). Vero E6 (*Cercopithecus aethiops* derived epithelial kidney cells, ATCC) cells were grown in Dulbecco's modified Eagle's medium (DMEM, Gibco) which was supplemented with 2.5% (v/v) fetal bovine serum (FBS, Gibco), 100 U/ml penicillin (PAN-

bioRxiv preprint doi: https://doi.org/10.1101/2020.10.15.340612; this version posted October 15, 2020. The copyright holder for this preprint (which was not certified by peer review) is the author/funder, who has granted bioRxiv a license to display the preprint in perpetuity. It is made available under aCC-BY-NC-ND 4.0 International license.

Biotech), 100 µg/ml Streptomycin (PAN-Biotech), 2 mM L-glutamine (PANBiotech), 1 mM sodium pyruvate (Gibco), and 1x non-essential amino acids (Gibco). All cells were cultured at 37°C in a 5% CO_2, 90% humidity atmosphere. Sendai Virus was a kind gift from Prof. Hans-Georg Koch, Institute for Biochemistry and Molecular Biology, University of Freiburg. Viral isolates BetaCoV/France/IDF0372/2020 (#014V-03890) and BetaCoV/Netherlands/01/NL/2020 (#010V-03903) were obtained through the European Virus Archive global.

Expression constructs and plasmids. pLVX-EF1alpha constructs containing all Strep II-tagged, codon optimized open reading frames (Orfs) of SARS-CoV-2 (control, Nsp1, Nsp2, Nsp3, Nsp4, Nsp5, Nsp6, Nsp7, Nsp8, Nsp9, Nsp10, Nsp11, Nsp12, Nsp13, Nsp14, Nsp15, Nsp16, S, ORF3a, ORF3c, E, M, ORF6, ORF7a, ORF7b, ORF8, N, ORF9b, ORF9c, and ORF10) were a kind gift by David Gordon and Nevan Krogan[39]. V5 tagged, codon optimized Orfs coding for Nsp1, Nsp3, Nsp7, Nsp15, M, N, ORF3a, ORF6, and ORF7a from SARS-CoV-2, RaTG13-CoV, and SARS-CoV-1 were synthesized by Twist Bioscience and subcloned into the pCG vector by restriction cloning using the restriction enzymes XbaI and MluI (New England Biolabs). Firefly luciferase reporter constructs harbouring binding sites for NF-κB or IRF3, ISRE or GAS sites, or the genomic promoter of IFNA4 or IFNB1 in front of the reporter were previously described[56,87]. The GAPDH_PROM_01 Renilla SP Luciferase construct was purchased from switchgear genomics. pCR3 constructs coding for FLAG-tagged Measles morbillivirus V (MeV V) protein or Rabies virus P (RABV P) protein were described previously[56,88]. pEGFP-N1_hTRIM32[89] was a gift from Martin Dorf (Addgene, #69541), the Orf of TRIM32 was subcloned into the pIRES_FLAG vector using Gibson assembly as previously described[42].

bioRxiv preprint doi: https://doi.org/10.1101/2020.10.15.340612; this version posted October 15, 2020. The copyright holder for this preprint (which was not certified by peer review) is the author/funder, who has granted bioRxiv a license to display the preprint in perpetuity. It is made available under aCC-BY-NC-ND 4.0 International license.

Transfections. Plasmid DNA was transfected using either the TransIT-LT1 Transfection Reagent (Mirus) or Polyethylenimine (PEI, 1 mg/ml in H_2O, Sigma-Aldrich) according to the manufacturers' recommendations or as described previously[42,90].

Luciferase assays. HEK293T cells were transiently transfected with Firefly luciferase reporter constructs, Renilla luciferase control constructs, and constructs expressing CoV Orfs in 48-well plates using TransIT-LT1. One day post-transfection, the cells were stimulated with IFN-β (1,000 U/ml, 8 h, Merck), IFN-α2 (500 U/ml, 24 h, Sigma-Aldrich), IFN-γ (400 U/ml, 24 h, Sigma-Aldrich), IFN-λ1 (100 ng/ml, 8 h, R&D Systems), IL-1α (10 ng/ml, 24 h , R&D Systems), TNFα (25 ng/ml , 24 h , Sigma-Aldrich), or SeV (1:500, 24 h, kindly provided by Hans-Georg Koch, Freiburg). 8-24 h post-stimulation, the cells were lysed in passive lysis buffer and luciferase activities of the Firefly luciferase and Renilla luciferase were determined using the Dual-Glo Luciferase Assay System (Promega) and an Orion II Microplate Luminometer (Berthold). Cell viability of the transfected cells was measured using the CellTiter-Glo Luminescent Cell Viability Assay (Promega).

Cell viability assay. Calu-3 or HEK293T cells were treated with cytokines or autophagy modulating drugs or transiently transfected using TransIT-LT1. To measure metabolic activity, cells were lysed in passive lysis buffer and analyzed using the CellTiter-Glo Luminescent Cell Viability Assay (Promega) according to manufacturer's instructions and an Orion II Microplate Luminometer (Berthold).

Autophagy quantification by flow cytometry. The number of autophagosomes was quantified as previously described[42], either in a basal state, or stimulated with Rapamycin (1 µM, Sigma) or Bafilomycin A1 (0.1 µM, Santa Cruz Biotechnology). In brief, HEK293T cells

bioRxiv preprint doi: https://doi.org/10.1101/2020.10.15.340612; this version posted October 15, 2020. The copyright holder for this preprint (which was not certified by peer review) is the author/funder, who has granted bioRxiv a license to display the preprint in perpetuity. It is made available under aCC-BY-NC-ND 4.0 International license.

564 stably expressing GFP-LC3B (HEK293T GL) were transiently transfected using PEI. 48 h
565 post-transfection, cells were harvested in PBS and treated for 20 min at 4 °C with PBS
566 containing 0.05% Saponin. Non-membrane bound GFP-LC3B was washed out of the
567 permeabilized cells using PBS (Gibco) twice, followed by fixation in 4% Paraformaldehyde
568 (PFA, Santa Cruz Biotechnology). The fluorescence intensity of membrane associated GFP-
569 LC3B was then quantified via flow cytometry (FACSCanto II, BD Biosciences). The GFP-
570 LC3B mean fluorescence intensity of the control (baseline) was subtracted.
571
572 **Whole-cell lysates.** Whole-cell lysates were prepared by collecting cells in Phosphate-
573 Buffered Saline (PBS). The cell pellet (500 g, 4 °C, 5 min) was lysed in transmembrane lysis
574 buffer [50 mM HEPES pH 7.4, 150 mM NaCl, 1% Triton X-100, 5 mM
575 ethylenediaminetetraacetic acid (EDTA)] by vortexing at maximum speed for 30 s. Cell debris
576 were pelleted by centrifugation (20,000 g, 4 °C, 20 min) and the total protein concentration of
577 the cleared lysates was measured using the Pierce BCA Protein Assay Kit (Thermo Scientific)
578 according to manufacturer's instructions. The lysates were adjusted to the same protein
579 concentration and stored at -20 °C.
580
581 **SDS-PAGE and immunoblotting.** SDS-PAGE and immunoblotting was performed using
582 standard techniques as previously described[42]. In brief, whole cell lysates were mixed with 6x
583 Protein Sample Loading Buffer (LI-COR, at a final dilution of 1x) supplemented with 15% β-
584 mercaptoethanol (Sigma Aldrich), heated to 95 °C for 5 min, separated on NuPAGE 4-12%
585 Bis-Tris Gels (Invitrogen) for 90 min at 100 V and blotted onto Immobilon-FL PVDF
586 membranes (Merck Millipore). The transfer was performed at a constant voltage of 30 V for
587 30 min. After the transfer, the membrane was blocked in 1% Casein in PBS (Thermo
588 Scientific). Proteins were stained using primary antibodies against β-actin (1:10,000, AC-15,

bioRxiv preprint doi: https://doi.org/10.1101/2020.10.15.340612; this version posted October 15, 2020. The copyright holder for this preprint (which was not certified by peer review) is the author/funder, who has granted bioRxiv a license to display the preprint in perpetuity. It is made available under aCC-BY-NC-ND 4.0 International license.

589 Sigma), Strep II-tag (1:1,000, NBP2-43735, Novus), Strep II-tag (1:2,000, ab76949, abcam),
590 GAPDH (1:1,000, 607902, Biologend), pSTAT1 (1:1,000, Y701, Cell Signaling Technology),
591 STAT1 (1:1,000, 9172S, Cell Signaling Technology), pSTAT2 (1:1,000, Y690, Cell Signaling
592 Technology), STAT2 (1:1,000, 4594S, Cell Signaling Technology), IFNAR1 (1:1,000,
593 ab45172, abcam), p62 (1:1,000, GP62-N, ProGen), LC3α/β (1:200, G-4, Santa Cruz
594 Biotechnology), Beclin-1 (1:1,000, 3738S, Cell Signaling Technology), ULK1 (1:1,000,
595 D8H5, Cell Signaling Technology), SARS-CoV-2 Nsp3 (1:1,000, GTX135614, GeneTex),
596 FLAG-tag (1:5,000, M2, Sigma), V5-tag (1:1,000, D3H8Q, Cell Signaling Technology),
597 SARS-CoV-2 (COVID-19) spike antibody (1:1000, 1A9, Biozol), SARS-CoV/SARS-CoV-2
598 Nucleocapsid Antibody (1:1000, MM05, SinoBiological), and Infrared Dye labelled secondary
599 antibodies (1:20,000, LI-COR IRDye), diluted in 0.05% Casein in PBS. Band intensities were
600 quantified using Image Studio (LI-COR) and protein levels were normalized on β-actin or
601 GAPDH levels.
602
603 **Immunofluorescence.** HeLa GL cells were transfected using TransIT-LT1 and grown on
604 coverslips in 24-well plates. The cells were fixed using 4% PFA, and permeabilized and
605 blocked with PBS containing 0.5% Triton X-100 (Sigma) and 5% FBS (Gibco). The cells were
606 stained using primary antibodies against Strep II-tag (1:200, NBP2-43735, Novus), V5-tag
607 (1:400, D3H8Q, Cell Signaling Technology), FLAG-tag (1:400, M2, Sigma) and TGN46
608 (1:400, AHP500GT, Bio Rad), secondary antibodies fluorescently labelled with
609 AlexaFluor568 targeting rabbit-IgGs (1:400, A10042, Invitrogen) and AlexaFluor647 targeting
610 sheep-IgG (1:400, A21448, Invitrogen), and DAPI (1:1,000, Sigma) to stain nuclei. The
611 coverslips were mounted on microscope slides using Mowiol mounting medium (10% (w/v)
612 Mowiol 4-88, 25% (w/v) Glycerol, 25% (v/v) water, 50% (v/v) Tris-HCl 0.2 M pH 8.5, 2.5%
613 (w/v) DABCO). Images were acquired using a Zeiss LSM710 and analysed with Fiji ImageJ.

bioRxiv preprint doi: https://doi.org/10.1101/2020.10.15.340612; this version posted October 15, 2020. The copyright holder for this preprint (which was not certified by peer review) is the author/funder, who has granted bioRxiv a license to display the preprint in perpetuity. It is made available under aCC-BY-NC-ND 4.0 International license.

Autophagy quantification by counting. HeLa GL cells were transfected using TransIT-LT1 and grown on coverslips in 24-well plates. The cells were treated and stained for the transfected proteins as described in the Immunofluorescence method-paragraph. After acquiring images of 30+ transfected cells, the total pixel area of GFP-LC3B puncta per cell was quantified using Fiji ImageJ as previously described[42]. In brief, the channels were separated to work with the GFP-channel, the background removed and smoothed, and a threshold was applied to isolate the GFP-LC3B puncta. By analysing the particles, the total area was determined. Cells treated with 1 µM chloroquine overnight were used as positive control.

RT-qPCR. SARS-CoV-2 N (nucleoprotein) transcript levels were determined as previously described[80,90]. In brief, supernatants were collected from SARS-CoV-2 infected Calu-3 cells 48 h post-infection. Total RNA was isolated using the Viral RNA Mini Kit (Qiagen, Cat# 52906) according to the manufacturer's instructions. RT-qPCR was performed as previously described using TaqMan Fast Virus 1-Step Master Mix (Thermo Fisher, Cat#4444436) and an OneStepPlus Real-Time PCR System (96-well format, fast mode). Primers were purchased from Biomers (Ulm, Germany) and dissolved in RNase free water. Synthetic SARS-CoV-2-RNA (Twist Bioscience) or RNA isolated from BetaCoV/France/IDF0372/2020 viral stocks quantified via this synthetic RNA (for low Ct samples) were used as a quantitative standard to obtain viral copy numbers. (Forward primer (HKU-NF): 5'-TAA TCA GAC AAG GAA CTG ATT A-3'; Reverse primer (HKU-NR): 5'-CGA AGG TGT GAC TTC CAT G-3'; Probe (HKU-NP): 5'-FAM-GCA AAT TGT GCA ATT TGC GG-TAMRA-3'.

Inhibition of SARS-CoV-2 by immune modulation. 300,000 Calu-3 cells were seeded in 12-well plates. The cells were stimulated with increasing amounts of IFNs (α2, β and γ, 0.8, 4, 20,

bioRxiv preprint doi: https://doi.org/10.1101/2020.10.15.340612; this version posted October 15, 2020. The copyright holder for this preprint (which was not certified by peer review) is the author/funder, who has granted bioRxiv a license to display the preprint in perpetuity. It is made available under aCC-BY-NC-ND 4.0 International license.

100 and 500 U/ml or λ1, 0.16, 0.8, 4, 20 and 100 ng/ml) at 24 h and 72 h post-seeding, with an intermediate medium change at 48 h post-seeding. 2 h after the second stimulation, the cells were infected with SARS-CoV-2 (MOI 0.05) and 6 h later the medium was changed. 48 h post-infection, the cells were harvested for further analysis.

Propagation of SARS-CoV-2. BetaCoV/Netherlands/01/NL/2020 and BetaCoV/ France/IDF0372/2020 were obtained from the European Virus Archive. The viruses were propagated by infecting 70% confluent Vero E6 in 75 cm^2 cell culture flasks at a MOI of 0.003 in 3.5 ml serum-free medium containing 1 µg/ml trypsin. The cells were then incubated for 2 h at 37 °C, before adding 20 ml medium containing 15 mM HEPES. Three days post-infection, the medium was exchanged and the supernatants were harvested 5 days post-infection upon visible cytopathic effect. The supernatants were cleared by centrifugation, aliquoted and stored at −80 °C. The infectious virus titre was determined as plaque forming units (PFU).

Proteome analysis. For the proteome analysis of infected cells, $0.6x10^6$ Caco-2 cells were infected with SARS-CoV-2 BetaCoV/Netherlands/01/NL/2020 at an MOI of 0.5 and harvested 24 h and 48 h post infection with WCL lysis buffer supplemented with 1:500 protease inhibitor. After centrifugation for 10 min with 14,000 rpm at 4 °C, the pellet was discarded. Then, the samples were boiled at 95 °C for 10 min to ensure denaturation. For the proteome analysis of single overexpressed SARS-CoV-2 proteins, $1x10^7$ HEK293T cells were transfected with the respective constructs (pCG vectors containing V5-tagged, codon optimized Orfs of SARS-CoV-2 (Nsp1, Nsp16, S, ORF3a, ORF7a)). The cells were harvested in PBS and processed for LC-MS using the iST-kit (Preomics) as recommended by the manufacturer. For LC-MS purposes, desalted peptides were injected in a nanoElute system (Bruker) and separated in a 25-cm analytical column (75 µm ID, 1.6 µm C18, IonOpticks) with a 100-min gradient from 2

bioRxiv preprint doi: https://doi.org/10.1101/2020.10.15.340612; this version posted October 15, 2020. The copyright holder for this preprint (which was not certified by peer review) is the author/funder, who has granted bioRxiv a license to display the preprint in perpetuity. It is made available under aCC-BY-NC-ND 4.0 International license.

664 to 37% acetonitrile in 0.1% formic acid. The effluent from the HPLC was directly
665 electrosprayed into a hybrid trapped ion mobility-quadrupole time-of-flight mass spectrometer
666 (timsTOF Pro, Bruker Daltonics, Bremen, Germany) using the nano-electrospray ion source at
667 1.4 kV (Captive Spray, Bruker Daltonics). The timsTOF was operated at 100% duty cycle in
668 data dependent mode to automatically switch between one full TIMS-MS scan and ten PASEF
669 MS/MS scans in the range from 100–1700 m/z in positive electrospray mode with an overall
670 acquisition cycle of 1.23 s. The ion mobility was scanned from 0.6 to 1.60 Vs/cm^2 with TIMS
671 ion charge control set to 5e4, RF potential of 300 Vpp. The TIMS dimension was calibrated
672 linearly using four selected ions from the Agilent ESI LC/MS tuning mix [m/z, 1/K0:
673 (322.0481, 0.7318 Vs/cm^2), (622.0289, 0.9848 Vs/cm^2), (922.0097, 1.1895 Vs/cm^2),
674 (1221.9906, 1.3820 Vs/cm^2)]. The mass spectrometry proteomics data have been deposited to
675 the ProteomeXchange Consortium via the PRIDE partner repository with the dataset identifier
676 PXD021899.MaxQuant 1.6.15.0 was used to identify proteins and quantify by LFQ with the
677 following parameters: Database, Uniprot_AUP000005640_Hsapiens_20200120.fasta
678 supplemented with the sequences of NSP1_V5, NSP7_V5, NSP15_V5, NSP16_V5, E_V5,
679 M_V5, N_V5, S_V5, ORF3_V5, ORF6_V5, ORF7_V5 and Spike protein from SARSCoV2[39];
680 MS tol, 10ppm; MS/MS tol, 20ppm Da; Peptide FDR, 0.1; Protein FDR, 0.01 Min. peptide
681 Length, 7; Variable modifications, Oxidation (M); Fixed modifications, Carbamidomethyl (C);
682 Peptides for protein quantitation, razor and unique; Min. peptides, 1; Min. ratio count, 2. Raw
683 data was analysed using R. Outliers (below 0.05 and above 0.95) appearing in more than 2
684 cases were removed. Heatmaps were generated using R, using the inbuilt hierarchical
685 clustering of heatmap.2 and displayed in Corel Draw.
686

bioRxiv preprint doi: https://doi.org/10.1101/2020.10.15.340612; this version posted October 15, 2020. The copyright holder for this preprint (which was not certified by peer review) is the author/funder, who has granted bioRxiv a license to display the preprint in perpetuity. It is made available under aCC-BY-NC-ND 4.0 International license.

GO Analysis. From the proteome of the respective samples, proteins regulated more than 4-fold compared to the vector control were extracted and submitted to PANTHER (cellular component analysis).

Half-life analysis. We focused on the half-life comparisons to proteins for which we identified peptides that resided within the first 50 N-terminal amino acids. To do this we extracted peptides for both NSP1+ (NSP over expression) and Vector (vector) samples that fall within the first 50 amino acid window starting at the N-terminus from the result file (peptide.txt, Maxquant 1.6.15.0). These peptides were then mapped to the corresponding protein intensities and the relative changes of log2 transformed iBAQ values calculated and grouped into three groups: I. enriched in NSP1+: $\log_2(fc) > 2$, II. enriched in Vector: $\log_2(fc) < -2$, III. Not enriched: $-2 <= \log_2(fc) <= 2$. The proteins for which data on the half lives in hepatocytes[47] were extracted and plotted by scaling their mean half-lives corresponding to the proteins in each group to the interval [0-1] using min-max normalization and generated boxplots for each of them. We used MATLAB 2019b for the half-life analysis.

Statistical analysis. Statistical analyses were performed using GraphPad PRISM 8 (GraphPad Software). P-values were determined using a two-tailed Student's t test with Welch's correction. Unless otherwise stated, data are shown as the mean of at least three biological replicates ± SEM. Significant differences are indicated as: *, $p < 0.05$; **, $p < 0.01$; ***, $p < 0.001$. Statistical parameters are specified in the figure legends.

REFERENCES

1. Zhou, P. *et al.* A pneumonia outbreak associated with a new coronavirus of probable bat

bioRxiv preprint doi: https://doi.org/10.1101/2020.10.15.340612; this version posted October 15, 2020. The copyright holder for this preprint (which was not certified by peer review) is the author/funder, who has granted bioRxiv a license to display the preprint in perpetuity. It is made available under aCC-BY-NC-ND 4.0 International license.

origin. *Nature* (2020) doi:10.1038/s41586-020-2012-7.

2. Wu, F. *et al.* A new coronavirus associated with human respiratory disease in China. *Nature* (2020) doi:10.1038/s41586-020-2008-3.

3. Andersen, K. G., Rambaut, A., Lipkin, W. I., Holmes, E. C. & Garry, R. F. The proximal origin of SARS-CoV-2. *Nature Medicine* (2020) doi:10.1038/s41591-020-0820-9.

4. Huang, C. *et al.* Clinical features of patients infected with 2019 novel coronavirus in Wuhan, China. *Lancet* (2020) doi:10.1016/S0140-6736(20)30183-5.

5. Ferretti, L. *et al.* Quantifying SARS-CoV-2 transmission suggests epidemic control with digital contact tracing. *Science (80-.).* (2020) doi:10.1126/science.abb6936.

6. WHO. Influenza and COVID-19 - similarities and differences. *World Health Organization* (2020).

7. Chan-yeung, M. & Xu, R. SARS : epidemiology CUMULATIVE NUMBER OF CASES AND DEATHS IN VARIOUS COUNTRIES IN. *Respirology* **8**, S9–S14 (2003).

8. Zumla, A., Hui, D. S. & Perlman, S. Middle East respiratory syndrome. *The Lancet* (2015) doi:10.1016/S0140-6736(15)60454-8.

9. Petersen, E. *et al.* Comparing SARS-CoV-2 with SARS-CoV and influenza pandemics. *Lancet Infect. Dis.* **20**, e238–e244 (2020).

10. Corman, V. M., Muth, D., Niemeyer, D. & Drosten, C. Hosts and Sources of Endemic Human Coronaviruses. in *Advances in Virus Research* (2018). doi:10.1016/bs.aivir.2018.01.001.

11. Kell, A. M. & Gale, M. RIG-I in RNA virus recognition. *Virology* (2015) doi:10.1016/j.virol.2015.02.017.

12. Totura, A. L. & Baric, R. S. SARS coronavirus pathogenesis: Host innate immune responses and viral antagonism of interferon. *Current Opinion in Virology* (2012) doi:10.1016/j.coviro.2012.04.004.

bioRxiv preprint doi: https://doi.org/10.1101/2020.10.15.340612; this version posted October 15, 2020. The copyright holder for this preprint (which was not certified by peer review) is the author/funder, who has granted bioRxiv a license to display the preprint in perpetuity. It is made available under aCC-BY-NC-ND 4.0 International license.

13. Frieman, M., Heise, M. & Baric, R. SARS coronavirus and innate immunity. *Virus Res.* (2008) doi:10.1016/j.virusres.2007.03.015.

14. Takeuchi, O. & Akira, S. Innate immunity to virus infection. *Immunological Reviews* (2009) doi:10.1111/j.1600-065X.2008.00737.x.

15. Koepke, L., Gack, M. U. & Sparrer, K. M. The antiviral activities of TRIM proteins. *Current Opinion in Microbiology* (2021) doi:10.1016/j.mib.2020.07.005.

16. Sparrer, K. M. J. & Gack, M. U. Intracellular detection of viral nucleic acids. *Current Opinion in Microbiology* (2015) doi:10.1016/j.mib.2015.03.001.

17. Van Gent, M., Sparrer, K. M. J. & Gack, M. U. TRIM proteins and their roles in antiviral host defenses. *Annu. Rev. Virol.* (2018) doi:10.1146/annurev-virology-092917-043323.

18. Shojaei, S., Suresh, M., Klionsky, D. J., Labouta, H. I. & Ghavami, S. Autophagy and SARS-CoV-2 infection: Apossible smart targeting of the autophagy pathway. *Virulence* (2020) doi:10.1080/21505594.2020.1780088.

19. Maier, H. J. & Britton, P. Involvement of autophagy in coronavirus replication. *Viruses* (2012) doi:10.3390/v4123440.

20. Sparrer, K. M. J. & Gack, M. U. TRIM proteins: New players in virus-induced autophagy. *PLoS Pathogens* (2018) doi:10.1371/journal.ppat.1006787.

21. Choi, Y., Bowman, J. W. & Jung, J. U. Autophagy during viral infection - A double-edged sword. *Nature Reviews Microbiology* (2018) doi:10.1038/s41579-018-0003-6.

22. Iwasaki, A. & Medzhitov, R. Regulation of adaptive immunity by the innate immune system. *Science* (2010) doi:10.1126/science.1183021.

23. Iwasaki, A. & Medzhitov, R. Control of adaptive immunity by the innate immune system. *Nature Immunology* (2015) doi:10.1038/ni.3123.

24. Zhang, Q. *et al.* Inborn errors of type I IFN immunity in patients with life-threatening COVID-

bioRxiv preprint doi: https://doi.org/10.1101/2020.10.15.340612; this version posted October 15, 2020. The copyright holder for this preprint (which was not certified by peer review) is the author/funder, who has granted bioRxiv a license to display the preprint in perpetuity. It is made available under aCC-BY-NC-ND 4.0 International license.

19. *Science (80-.).* eabd4570 (2020) doi:10.1126/science.abd4570.

25. Bastard, P. *et al.* Auto-antibodies against type I IFNs in patients with life-threatening COVID-19. *Science (80-.).* (2020) doi:10.1126/science.abd4585.

26. Lokugamage, K. *et al.* Type I interferon susceptibility distinguishes SARS-CoV-2 from SARS-CoV. *bioRxiv Prepr. Serv. Biol.* (2020) doi:10.1101/2020.03.07.982264.

27. Stukalov, A. *et al.* Multi-level proteomics reveals host-perturbation strategies of SARS-CoV-2 and SARS-CoV. *bioRxiv* (2020) doi:10.1101/2020.06.17.156455.

28. Blanco-Melo, D. *et al.* Imbalanced Host Response to SARS-CoV-2 Drives Development of COVID-19. *Cell* (2020) doi:10.1016/j.cell.2020.04.026.

29. Konno, Y. *et al.* SARS-CoV-2 ORF3b Is a Potent Interferon Antagonist Whose Activity Is Increased by a Naturally Occurring Elongation Variant. *Cell Rep.* (2020) doi:10.1016/j.celrep.2020.108185.

30. Thoms, M. *et al.* Structural basis for translational shutdown and immune evasion by the Nsp1 protein of SARS-CoV-2. *Science (80-.).* (2020) doi:10.1126/science.abc8665.

31. Lei, X. *et al.* Activation and evasion of type I interferon responses by SARS-CoV-2. *Nat. Commun.* (2020) doi:10.1038/s41467-020-17665-9.

32. Xia, H. *et al.* Evasion of Type I Interferon by SARS-CoV-2. *Cell Rep.* 108234 (2020) doi:10.1016/j.celrep.2020.108234.

33. Addetia, A. *et al.* SARS-CoV-2 ORF6 disrupts nucleocytoplasmic transport through interactions with Rae1 and Nup98. *bioRxiv* (2020) doi:10.1101/2020.08.03.234559.

34. Fragkou, P. C. *et al.* Review of trials currently testing treatment and prevention of COVID-19. *Clinical Microbiology and Infection* (2020) doi:10.1016/j.cmi.2020.05.019.

35. Van Zonneveld, M. *et al.* The safety of pegylated interferon alpha-2b in the treatment of chronic hepatitis B: Predictive factors for dose reduction and treatment discontinuation.

bioRxiv preprint doi: https://doi.org/10.1101/2020.10.15.340612; this version posted October 15, 2020. The copyright holder for this preprint (which was not certified by peer review) is the author/funder, who has granted bioRxiv a license to display the preprint in perpetuity. It is made available under aCC-BY-NC-ND 4.0 International license.

Aliment. Pharmacol. Ther. (2005) doi:10.1111/j.1365-2036.2005.02453.x.

36. Neri, S. *et al.* A Multidisciplinary Therapeutic Approach for Reducing the Risk of Psychiatric Side Effects in Patients With Chronic Hepatitis C Treated With Pegylated Interferon α and Ribavirin. *J. Clin. Gastroenterol.* (2010) doi:10.1097/MCG.0b013e3181d88af5.

37. Fried, M. W. Side effects of therapy of hepatitis C and their management. in *Hepatology* (2002). doi:10.1053/jhep.2002.36810.

38. Hung, I. F. N. *et al.* Triple combination of interferon beta-1b, lopinavir–ritonavir, and ribavirin in the treatment of patients admitted to hospital with COVID-19: an open-label, randomised, phase 2 trial. *Lancet* (2020) doi:10.1016/S0140-6736(20)31042-4.

39. Gordon, D. E. *et al.* A SARS-CoV-2 protein interaction map reveals targets for drug repurposing. *Nature* (2020) doi:10.1038/s41586-020-2286-9.

40. Hachim, A. *et al.* ORF8 and ORF3b antibodies are accurate serological markers of early and late SARS-CoV-2 infection. *Nat. Immunol.* (2020) doi:10.1038/s41590-020-0773-7.

41. Klionsky, D. J. *et al.* Guidelines for the use and interpretation of assays for monitoring autophagy (3rd edition). *Autophagy* (2016) doi:10.1080/15548627.2015.1100356.

42. Koepke, L. *et al.* An improved method for high-throughput quantification of autophagy in mammalian cells. *Sci. Rep.* (2020) doi:10.1038/s41598-020-68607-w.

43. Lei, X. *et al.* Activation and evasion of type I interferon responses by SARS-CoV-2. *Nat. Commun.* **11**, 1–12 (2020).

44. Yuen, C. K. *et al.* SARS-CoV-2 nsp13, nsp14, nsp15 and orf6 function as potent interferon antagonists. *Emerg. Microbes Infect.* **9**, 1418–1428 (2020).

45. Russell, R. C. *et al.* ULK1 induces autophagy by phosphorylating Beclin-1 and activating VPS34 lipid kinase. *Nat. Cell Biol.* (2013) doi:10.1038/ncb2757.

46. Wang, C. W. & Klionsky, D. J. The molecular mechanism of autophagy. *Molecular Medicine*

bioRxiv preprint doi: https://doi.org/10.1101/2020.10.15.340612; this version posted October 15, 2020. The copyright holder for this preprint (which was not certified by peer review) is the author/funder, who has granted bioRxiv a license to display the preprint in perpetuity. It is made available under aCC-BY-NC-ND 4.0 International license.

(2003) doi:10.1007/bf03402040.

47. Mathieson, T. *et al.* Systematic analysis of protein turnover in primary cells. *Nat. Commun.* (2018) doi:10.1038/s41467-018-03106-1.

48. Brandizzi, F. & Barlowe, C. Organization of the ER-Golgi interface for membrane traffic control. *Nature Reviews Molecular Cell Biology* (2013) doi:10.1038/nrm3588.

49. Progida, C. & Bakke, O. Bidirectional traffic between the Golgi and the endosomes - machineries and regulation. *Journal of Cell Science* (2016) doi:10.1242/jcs.185702.

50. Hansen, M. D. *et al.* Hepatitis C virus triggers Golgi fragmentation and autophagy through the immunity-related GTPase M. *Proc. Natl. Acad. Sci. U. S. A.* (2017) doi:10.1073/pnas.1616683114.

51. Freundt, E. C. *et al.* The Open Reading Frame 3a Protein of Severe Acute Respiratory Syndrome-Associated Coronavirus Promotes Membrane Rearrangement and Cell Death. *J. Virol.* (2010) doi:10.1128/jvi.01662-09.

52. Tao, Y., Yang, Y., Zhou, R. & Gong, T. Golgi Apparatus: An Emerging Platform for Innate Immunity. *Trends in Cell Biology* (2020) doi:10.1016/j.tcb.2020.02.008.

53. Rieder, M. & Conzelmann, K. K. Rhabdovirus evasion of the interferon system. *Journal of Interferon and Cytokine Research* (2009) doi:10.1089/jir.2009.0068.

54. Brzózka, K., Finke, S. & Conzelmann, K.-K. Inhibition of Interferon Signaling by Rabies Virus Phosphoprotein P: Activation-Dependent Binding of STAT1 and STAT2. *J. Virol.* (2006) doi:10.1128/jvi.80.6.2675-2683.2006.

55. Brzózka, K., Finke, S. & Conzelmann, K.-K. Identification of the Rabies Virus Alpha/Beta Interferon Antagonist: Phosphoprotein P Interferes with Phosphorylation of Interferon Regulatory Factor 3. *J. Virol.* (2005) doi:10.1128/jvi.79.12.7673-7681.2005.

56. Sparrer, K. M. J., Pfaller, C. K. & Conzelmann, K.-K. Measles Virus C Protein Interferes with

bioRxiv preprint doi: https://doi.org/10.1101/2020.10.15.340612; this version posted October 15, 2020. The copyright holder for this preprint (which was not certified by peer review) is the author/funder, who has granted bioRxiv a license to display the preprint in perpetuity. It is made available under aCC-BY-NC-ND 4.0 International license.

Beta Interferon Transcription in the Nucleus. *J. Virol.* (2012) doi:10.1128/jvi.05899-11.

57. Takeuchi, K., Kadota, S. I., Takeda, M., Miyajima, N. & Nagata, K. Measles virus V protein blocks interferon (IFN)-α/β but not IFN-γ signaling by inhibiting STAT1 and STAT2 phosphorylation. *FEBS Lett.* (2003) doi:10.1016/S0014-5793(03)00528-3.

58. Palosaari, H., Parisien, J.-P., Rodriguez, J. J., Ulane, C. M. & Horvath, C. M. STAT Protein Interference and Suppression of Cytokine Signal Transduction by Measles Virus V Protein. *J. Virol.* (2003) doi:10.1128/jvi.77.13.7635-7644.2003.

59. Yang, Q. *et al.* TRIM32-TAX1BP1-dependent selective autophagic degradation of TRIF negatively regulates TLR3/4-mediated innate immune responses. *PLoS Pathog.* (2017) doi:10.1371/journal.ppat.1006600.

60. Overå, K. S. *et al.* TRIM32, but not its muscular dystrophy-associated mutant, positively regulates and is targeted to autophagic degradation by p62/SQSTM1. *J. Cell Sci.* (2019) doi:10.1242/jcs.236596.

61. Levine, B., Mizushima, N. & Virgin, H. W. Autophagy in immunity and inflammation. *Nature* (2011) doi:10.1038/nature09782.

62. Deretic, V., Saitoh, T. & Akira, S. Autophagy in infection, inflammation and immunity. *Nature Reviews Immunology* (2013) doi:10.1038/nri3532.

63. Matsuzawa-Ishimoto, Y., Hwang, S. & Cadwell, K. Autophagy and Inflammation. *Annual Review of Immunology* (2018) doi:10.1146/annurev-immunol-042617-053253.

64. Chiang, J. J. *et al.* Viral unmasking of cellular 5S rRNA pseudogene transcripts induces RIG-I-mediated immunity article. *Nat. Immunol.* (2018) doi:10.1038/s41590-017-0005-y.

65. Sparrer, K. M. J. *et al.* TRIM23 mediates virus-induced autophagy via activation of TBK1. *Nat. Microbiol.* (2017) doi:10.1038/s41564-017-0017-2.

66. Padhan, K. *et al.* Severe acute respiratory syndrome coronavirus Orf3a protein interacts with

bioRxiv preprint doi: https://doi.org/10.1101/2020.10.15.340612; this version posted October 15, 2020. The copyright holder for this preprint (which was not certified by peer review) is the author/funder, who has granted bioRxiv a license to display the preprint in perpetuity. It is made available under aCC-BY-NC-ND 4.0 International license.

caveolin. *J. Gen. Virol.* (2007) doi:10.1099/vir.0.82856-0.

67. Kagan, J. C. Signaling organelles of the innate immune system. *Cell* (2012) doi:10.1016/j.cell.2012.11.011.

68. Baez-Santos, Y. M., Mielech, A. M., Deng, X., Baker, S. & Mesecar, A. D. Catalytic Function and Substrate Specificity of the Papain-Like Protease Domain of nsp3 from the Middle East Respiratory Syndrome Coronavirus. *J. Virol.* (2014) doi:10.1128/jvi.01294-14.

69. Lei, J., Kusov, Y. & Hilgenfeld, R. Nsp3 of coronaviruses: Structures and functions of a large multi-domain protein. *Antiviral Research* (2018) doi:10.1016/j.antiviral.2017.11.001.

70. Shin, D. *et al.* Papain-like protease regulates SARS-CoV-2 viral spread and innate immunity. *Nature* (2020) doi:10.1038/s41586-020-2601-5.

71. Stobart, C. C. *et al.* Chimeric Exchange of Coronavirus nsp5 Proteases (3CLpro) Identifies Common and Divergent Regulatory Determinants of Protease Activity. *J. Virol.* (2013) doi:10.1128/jvi.02050-13.

72. Muramatsu, T. *et al.* SARS-CoV 3CL protease cleaves its C-terminal autoprocessing site by novel subsite cooperativity. *Proc. Natl. Acad. Sci. U. S. A.* (2016) doi:10.1073/pnas.1601327113.

73. Ivanov, K. A. & Ziebuhr, J. Human Coronavirus 229E Nonstructural Protein 13: Characterization of Duplex-Unwinding, Nucleoside Triphosphatase, and RNA 5′-Triphosphatase Activities. *J. Virol.* (2004) doi:10.1128/jvi.78.14.7833-7838.2004.

74. Shu, T. *et al.* SARS-Coronavirus-2 Nsp13 Possesses NTPase and RNA Helicase Activities That Can Be Inhibited by Bismuth Salts. *Virol. Sin.* (2020) doi:10.1007/s12250-020-00242-1.

75. Deng, X. & Baker, S. C. An “Old” protein with a new story: Coronavirus endoribonuclease is important for evading host antiviral defenses. *Virology* (2018) doi:10.1016/j.virol.2017.12.024.

76. Seyran, M. *et al.* Questions concerning the proximal origin of SARS-CoV-2. *J. Med. Virol.*

bioRxiv preprint doi: https://doi.org/10.1101/2020.10.15.340612; this version posted October 15, 2020. The copyright holder for this preprint (which was not certified by peer review) is the author/funder, who has granted bioRxiv a license to display the preprint in perpetuity. It is made available under aCC-BY-NC-ND 4.0 International license.

(2020) doi:10.1002/jmv.26478.

77. Zhang, T., Wu, Q. & Zhang, Z. Probable Pangolin Origin of SARS-CoV-2 Associated with the COVID-19 Outbreak. *Curr. Biol.* (2020) doi:10.1016/j.cub.2020.03.022.

78. Lam, T. T. Y. *et al.* Identifying SARS-CoV-2-related coronaviruses in Malayan pangolins. *Nature* (2020) doi:10.1038/s41586-020-2169-0.

79. Ribero, M. S., Jouvenet, N., Dreux, M. & Nisole, S. Interplay between SARS-CoV-2 and the type I interferon response. *PLoS Pathogens* (2020) doi:10.1371/journal.ppat.1008737.

80. Nchioua, R. *et al. The Zinc Finger Antiviral Protein restricts SARS-CoV-2*. *bioRxiv* (2020). doi:10.1101/2020.06.04.134379.

81. Hadjadj, J. *et al.* Impaired type I interferon activity and inflammatory responses in severe COVID-19 patients. *Science (80-.).* (2020) doi:10.1126/science.abc6027.

82. Tay, M. Z., Poh, C. M., Rénia, L., MacAry, P. A. & Ng, L. F. P. The trinity of COVID-19: immunity, inflammation and intervention. *Nature Reviews Immunology* (2020) doi:10.1038/s41577-020-0311-8.

83. Chen, G. *et al.* Clinical and immunological features of severe and moderate coronavirus disease 2019. *J. Clin. Invest.* (2020) doi:10.1172/JCI137244.

84. Sette, A. & Crotty, S. Pre-existing immunity to SARS-CoV-2: the knowns and unknowns. *Nature Reviews Immunology* (2020) doi:10.1038/s41577-020-0389-z.

85. Le Bert, N. *et al.* SARS-CoV-2-specific T cell immunity in cases of COVID-19 and SARS, and uninfected controls. *Nature* (2020) doi:10.1038/s41586-020-2550-z.

86. Sleijfer, S., Bannink, M., Van Gool, A. R., Kruit, W. H. J. & Stoter, G. Side effects of interferon-α therapy. *Pharmacy World and Science* (2005) doi:10.1007/s11096-005-1319-7.

87. Pfaller, C. K. & Conzelmann, K.-K. Measles Virus V Protein Is a Decoy Substrate for IκB Kinase α and Prevents Toll-Like Receptor 7/9-Mediated Interferon Induction. *J. Virol.* (2008)

bioRxiv preprint doi: https://doi.org/10.1101/2020.10.15.340612; this version posted October 15, 2020. The copyright holder for this preprint (which was not certified by peer review) is the author/funder, who has granted bioRxiv a license to display the preprint in perpetuity. It is made available under aCC-BY-NC-ND 4.0 International license.

904 doi:10.1128/jvi.01321-08.

905 88. Langer, S. *et al.* Hiv-1 vpu is a potent transcriptional suppressor of nf-kb-elicited antiviral
906 immune responses. *Elife* (2019) doi:10.7554/eLife.41930.

907 89. Fu, B. *et al.* TRIM32 Senses and Restricts Influenza A Virus by Ubiquitination of PB1
908 Polymerase. *PLoS Pathog.* (2015) doi:10.1371/journal.ppat.1004960.

909 90. Bozzo, C. P. *et al.* IFITM proteins promote SARS-CoV-2 infection of human lung cells.
910 *bioRxiv* (2020) doi:10.1101/2020.08.18.255935.

911

bioRxiv preprint doi: https://doi.org/10.1101/2020.10.15.340612; this version posted October 15, 2020. The copyright holder for this preprint (which was not certified by peer review) is the author/funder, who has granted bioRxiv a license to display the preprint in perpetuity. It is made available under aCC-BY-NC-ND 4.0 International license.

Figure 1

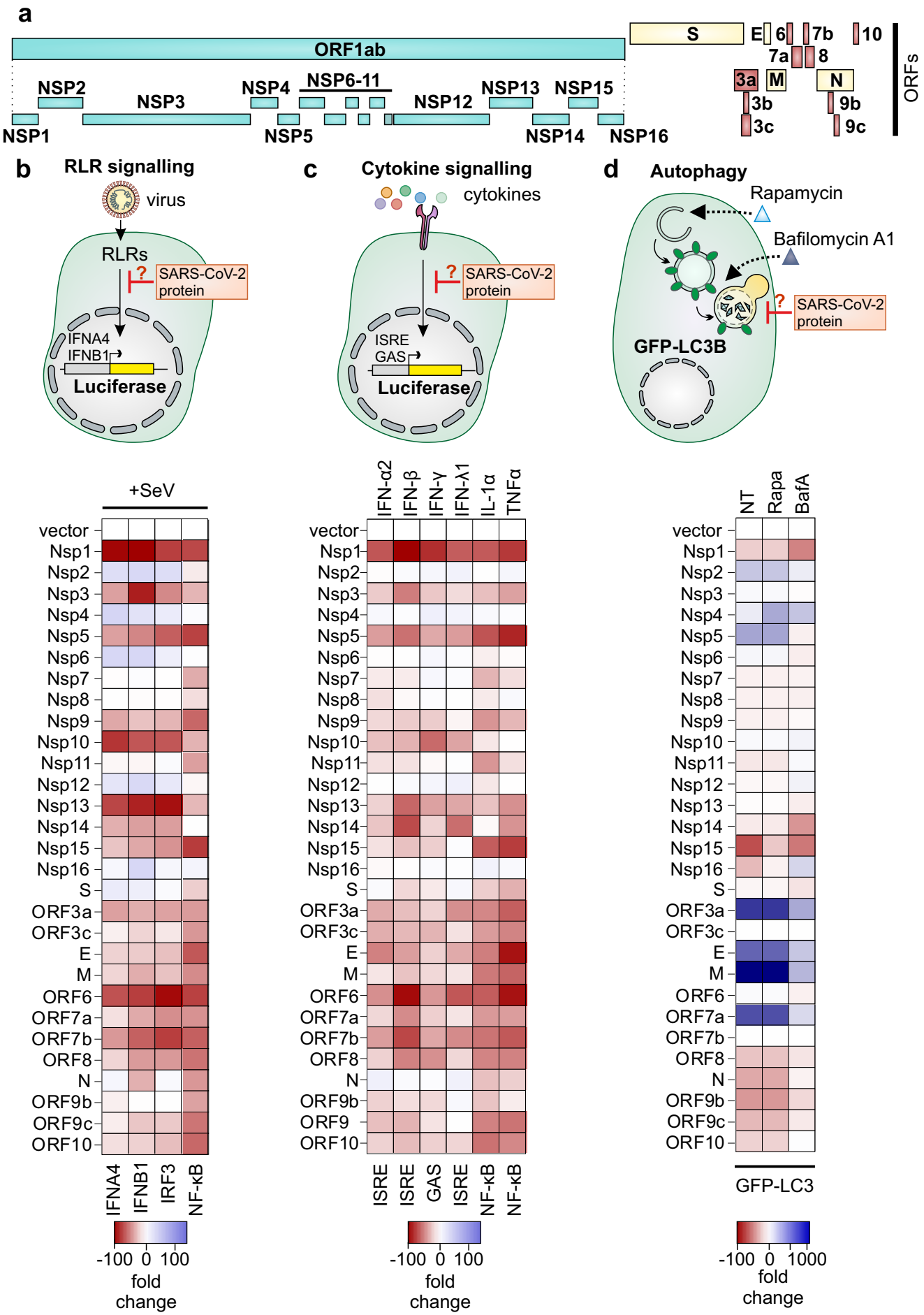

bioRxiv preprint doi: https://doi.org/10.1101/2020.10.15.340612; this version posted October 15, 2020. The copyright holder for this preprint (which was not certified by peer review) is the author/funder, who has granted bioRxiv a license to display the preprint in perpetuity. It is made available under aCC-BY-NC-ND 4.0 International license.

Figure 2

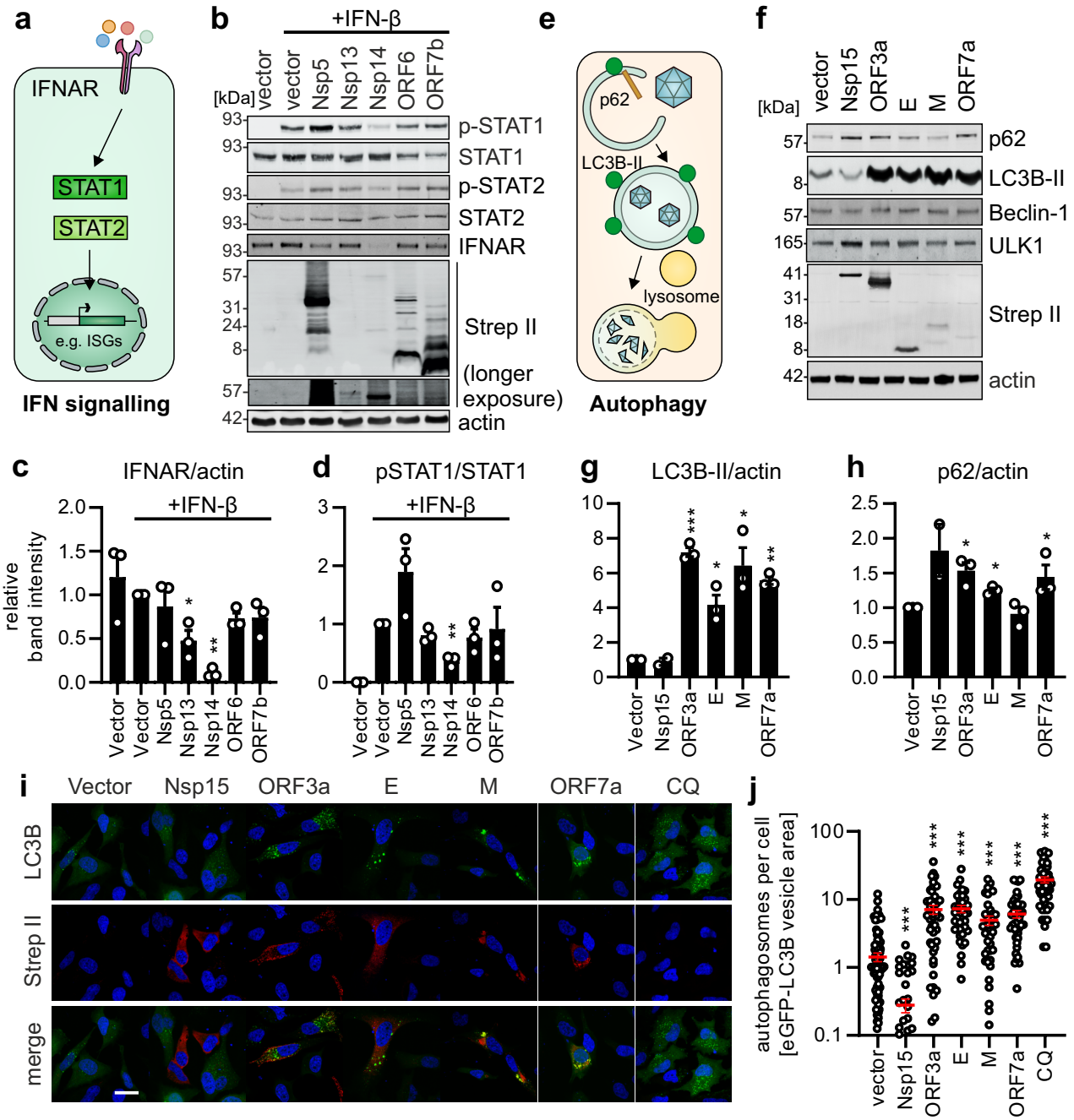

bioRxiv preprint doi: https://doi.org/10.1101/2020.10.15.340612; this version posted October 15, 2020. The copyright holder for this preprint (which was not certified by peer review) is the author/funder, who has granted bioRxiv a license to display the preprint in perpetuity. It is made available under aCC-BY-NC-ND 4.0 International license.

Figure 3

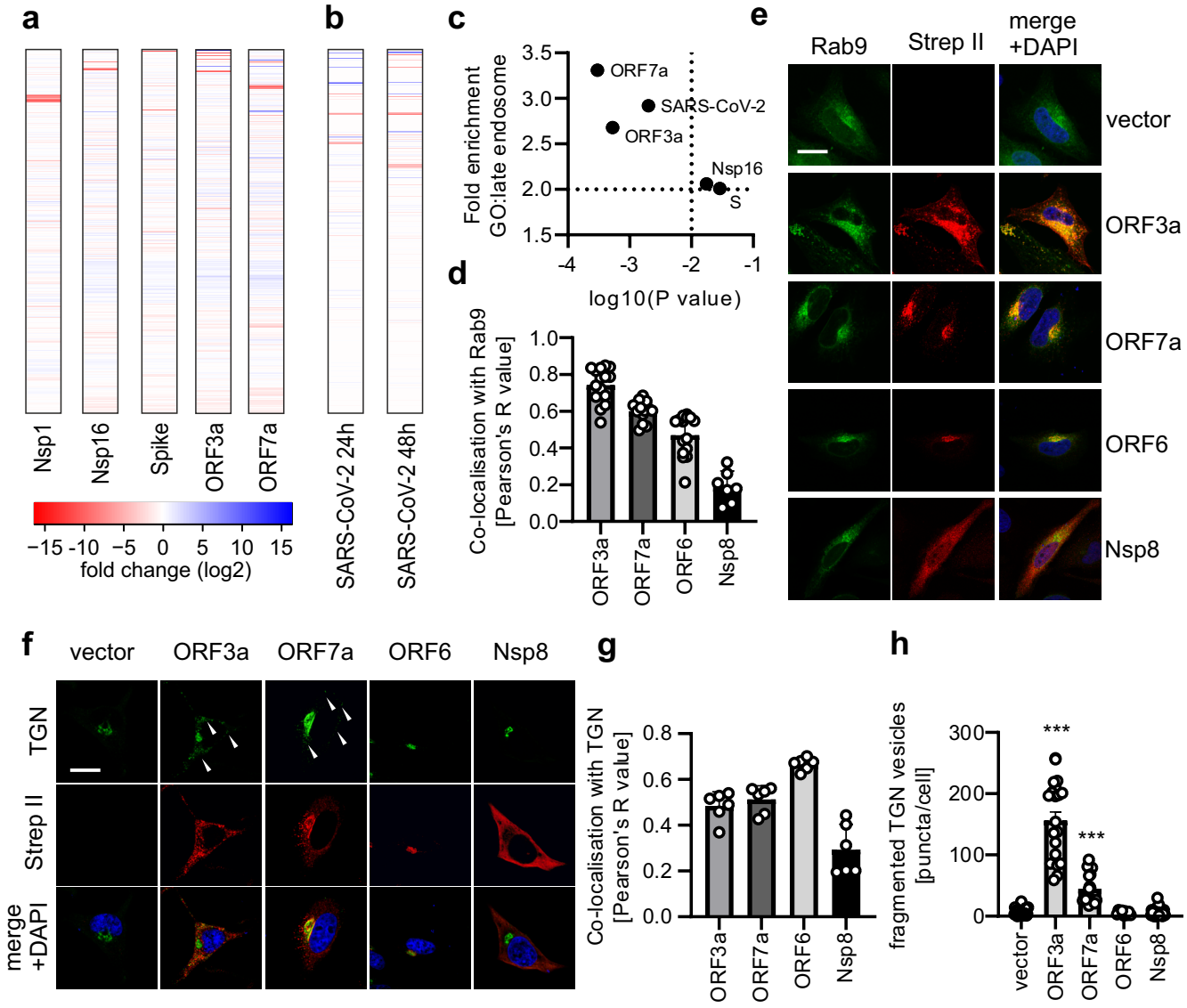

bioRxiv preprint doi: https://doi.org/10.1101/2020.10.15.340612; this version posted October 15, 2020. The copyright holder for this preprint (which was not certified by peer review) is the author/funder, who has granted bioRxiv a license to display the preprint in perpetuity. It is made available under aCC-BY-NC-ND 4.0 International license.

Figure 4

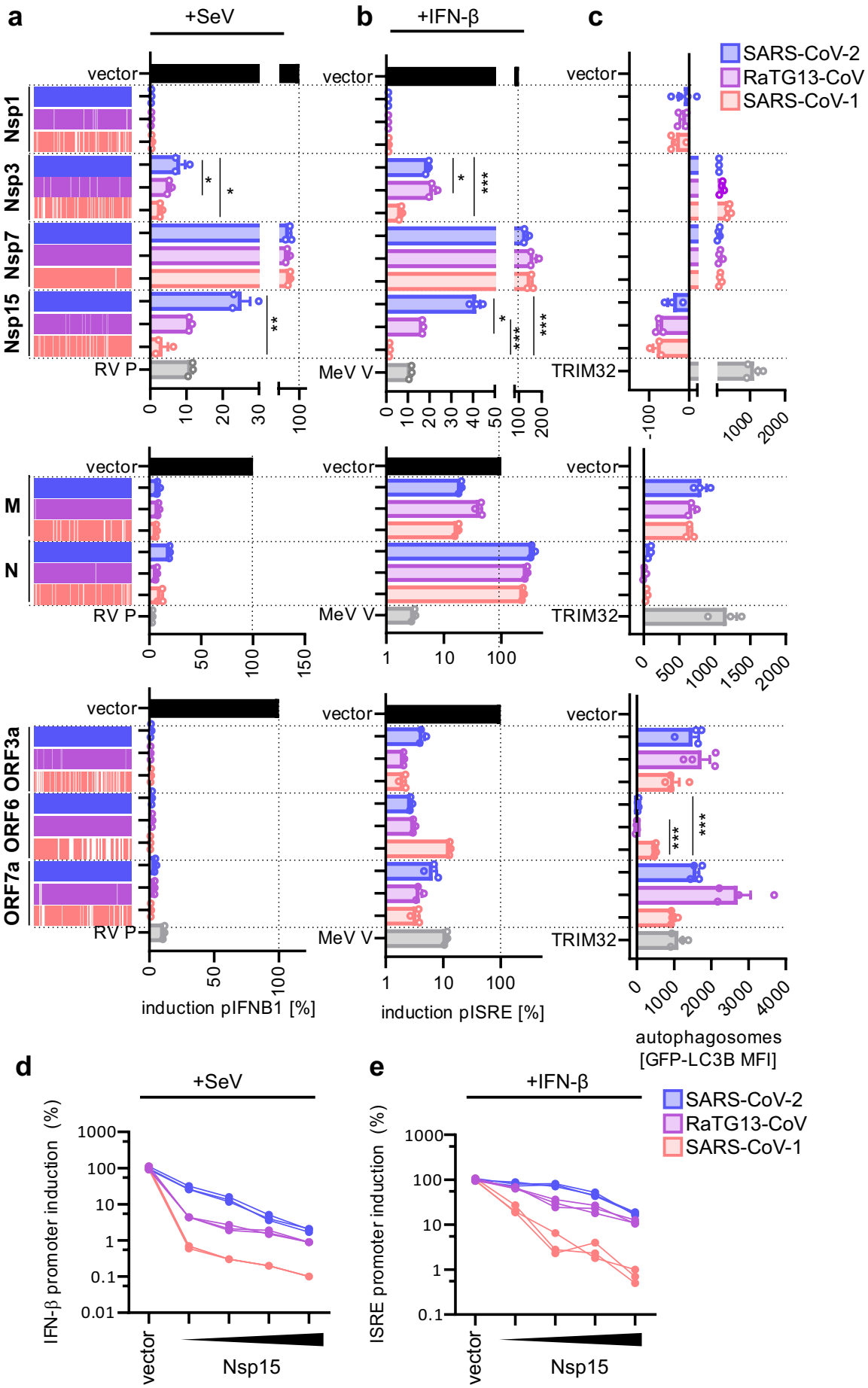

bioRxiv preprint doi: https://doi.org/10.1101/2020.10.15.340612; this version posted October 15, 2020. The copyright holder for this preprint (which was not certified by peer review) is the author/funder, who has granted bioRxiv a license to display the preprint in perpetuity. It is made available under aCC-BY-NC-ND 4.0 International license.

Figure 5